BIOCHEMISTRY

Adult-onset obesity is triggered by impaired mitochondrial gene expression

Kara L. Perks,[1] Nicola Ferreira,[1] Tara R. Richman,[1] Judith A. Ermer,[1] Irina Kuznetsova,[1] Anne-Marie J. Shearwood,[1] Richard G. Lee,[1] Helena M. Viola,[2] Victoria P. A. Johnstone,[2] Vance Matthews,[3] Livia C. Hool,[2,4] Oliver Rackham,[1,5] Aleksandra Filipovska[1,5]*

Mitochondrial gene expression is essential for energy production; however, an understanding of how it can influence physiology and metabolism is lacking. Several proteins from the pentatricopeptide repeat (PPR) family are essential for the regulation of mitochondrial gene expression, but the functions of the remaining members of this family are poorly understood. We created knockout mice to investigate the role of the PPR domain 1 (PTCD1) protein and show that loss of PTCD1 is embryonic lethal, whereas haploinsufficient, heterozygous mice develop age-induced obesity. The molecular defects and metabolic consequences of mitochondrial protein haploinsufficiency in vivo have not been investigated previously. We show that PTCD1 haploinsufficiency results in increased RNA metabolism, in response to decreased protein synthesis and impaired RNA processing that affect the biogenesis of the respiratory chain, causing mild uncoupling and changes in mitochondrial morphology. We demonstrate that with age, these effects lead to adult-onset obesity that results in liver steatosis and cardiac hypertrophy in response to tissue-specific differential regulation of the mammalian target of rapamycin pathways. Our findings indicate that changes in mitochondrial gene expression have long-term consequences on energy metabolism, providing evidence that haploinsufficiency of PTCD1 can be a major predisposing factor for the development of metabolic syndrome.

INTRODUCTION

Mitochondria provide most of the energy required for life via oxidative phosphorylation (OXPHOS), making them essential for cell function. The endosymbiotic origin of these organelles has resulted in their dependence on two genomes for their biogenesis, the nuclear genome and mitochondrial DNA (mtDNA) contained within each mitochondrion. mtDNA codes for 13 polypeptides that are members of the OXPHOS system, along with 22 transfer RNAs (tRNAs) and 2 ribosomal RNAs (rRNAs), all of which are required for their synthesis. The remaining nuclear-encoded proteins are translated on cytoplasmic ribosomes and imported into mitochondria co- or posttranscriptionally. Therefore, the biogenesis of the OXPHOS system and energy production relies on coordinated regulation of mitochondrial and nuclear gene expression. The expression of mtDNA is regulated predominantly at the post-transcriptional level by RNA-binding proteins that are involved in RNA processing, stability, maturation, translation, and degradation [reviewed by Rackham *et al.* (*1*) and Hällberg and Larsson (*2*)]. An increasing number of mitochondrial proteins have been identified that affect RNA metabolism and protein synthesis; however, their molecular function, effects on antero- and retrograde cell signaling, and physiological consequences of their loss in vivo are still poorly characterized.

Genetic modifications and environmental signals, including diet, can alter mitochondrial fat and carbohydrate metabolism by causing defects in mitochondrial transcripts or mitochondrial proteins that lead to mitochondrial dysfunction and consequently diminished energy production, a major symptom of many inherited diseases (*3*). There is a major gap in our understanding about how impaired mitochondrial gene expression can have downstream or retrograde effects on cell signaling and the physiology of different tissues within an organism. Because mitochondrial RNA-binding proteins (mt-RBPs) are nuclear-encoded and crucial for the regulation of mitochondrial RNA (mt-RNA) metabolism, there is a need to investigate how their expression or loss affects both mitochondrial and cellular function in vivo.

The pentatricopeptide repeat (PPR) proteins are a family of RNA-binding proteins that has recently attracted considerable interest in the gene expression field because of the sequence-specific recognition of their RNA targets (*4*, *5*). The PPR proteins in eukaryotes have versatile regulatory roles in gene expression within organelles ranging from transcription, RNA splicing, processing, editing, and translation (*6*). In mammals, there are only seven PPR proteins, all of which are mitochondrial, each with different roles in posttranscriptional regulation of mitochondrial gene expression, including transcription, processing, stability, and translation [reviewed by Rackham and Filipovska (*7*)]. Although the roles of the mitochondrial RNA polymerase (POLRMT) in transcription, the ribonuclease (RNase) P subunit MRPP3 in processing and ribosome assembly, LRPPRC in polyadenylation and translation, and the two small ribosomal subunit proteins PTCD3 and MRPS27 have been investigated previously (*8*–*14*), less is known about the PPR domain 1 (PTCD1) and PTCD2 proteins (*15*, *16*).

Initially, we identified PTCD1 as a mitochondrial matrix protein that regulates mitochondrial gene expression in cells (*16*). Knockdown of PTCD1 affected the processing of mitochondrial tRNAs (mt-tRNAs) required for mitochondrial biogenesis and energy production (*16*). We also found PTCD1 associated with the mitochondrial RNase Z or ELAC2 protein (*17*), further suggesting that it may be involved in mt-RNA processing. To understand the role of PTCD1 in vivo, we created a constitutive knockout of the *Ptcd1* gene in mice, enabling us to understand how its loss could affect mitochondrial and cell function. The homozygous knockout of *Ptcd1* is embryonic lethal, whereas the

[1]Harry Perkins Institute of Medical Research, Centre for Medical Research, QEII Medical Centre, University of Western Australia, Nedlands, Western Australia 6009, Australia. [2]School of Human Sciences, University of Western Australia, Crawley, Western Australia 6009, Australia [3]School of Biomedical Sciences, University of Western Australia, Crawley, Western Australia 6009, Australia. [4]Victor Chang Cardiac Research Institute, Darlinghurst, New South Wales 2010, Australia. [5]School of Molecular Sciences, University of Western Australia, Crawley, Western Australia 6009, Australia.
*Corresponding author. Email: aleksandra.filipovska@uwa.edu.au

heterozygous mice are haploinsufficient for PTCD1 and develop adult-onset obesity, providing a model to investigate in vivo how impaired mitochondrial gene expression leads to the development of metabolic syndrome.

Haploinsufficiency of PTCD1 leads to decreased protein synthesis, affects RNA processing, and results in decreased complex biogenesis, reduced oxygen consumption, and uncoupling of OXPHOS. Reduction of PTCD1 with age causes an accumulation of the short form of OPA1 and decreased membrane potential and consequently affects the morphology of mitochondria and cristae formation. The characterization of the molecular and functional changes as a result of decreased PTCD1 levels with age reveals a novel role for this protein in metabolic dysfunction and age-onset obesity through retrograde tissue-specific mammalian target of rapamycin (mTOR) signaling via adenosine monophosphate–activated protein kinase (AMPK). The heterozygous ($Ptcd1^{+/-}$) mice undergo a metabolic switch with age as a result of lowered energy capacity and alterations in metabolic hormones, growth factors, and proinflammatory cytokines, which causes tissue-specific molecular and pathological changes, leading to late-onset hypertrophy in the heart, hepatic steatosis, and obesity.

RESULTS

PTCD1 is required for balanced mt-RNA metabolism

PTCD1 has an N-terminal mitochondrial targeting signal that localizes it to the matrix and at least eight PPRs that play a role in its association with RNA (*16*, *18*). To understand the in vivo role of PTCD1, we generated a knockout allele of the mouse *Ptcd1* gene in embryonic stem (ES) cells (fig. S1A) and subsequent transmission through the germ line to obtain heterozygous $Ptcd1^{+/-}$ animals. Intercrossing $Ptcd1^{+/-}$ mice produced $Ptcd1^{+/-}$ and $Ptcd1^{+/+}$ mice in Mendelian proportions (genotyped pups, $n = 629$; $Ptcd1^{+/-}$, $n = 402$; and $Ptcd1^{+/+}$, $n = 227$); however, the homozygous knockout mice ($Ptcd1^{-/-}$) were not viable. Analyses of essential proteins involved in mitochondrial gene expression have shown embryonic lethality at embryonic day 8.5 (E8.5) (*13*, *19*–*23*); therefore, we analyzed the embryos at this stage to identify that $Ptcd1^{-/-}$ embryos had not developed normally compared to those observed for $Ptcd1^{+/+}$ and $Ptcd1^{+/-}$ mice, and hence, the loss of PTCD1 was embryonic lethal (fig. S1B). Therefore, we conclude that PTCD1 is essential for embryo development and survival, much like the other three mammalian PPR proteins knocked out in mice to date: POLRMT (*11*), MRPP3 (*12*), and LRPPRC (*13*).

The $Ptcd1^{+/-}$ mice develop normally; both male and female mice were fertile and their survival was similar to their wild-type littermates. However, we observed that by 30 weeks of age, the $Ptcd1^{+/-}$ mice appeared obese (Fig. 1A) and were significantly heavier compared to their $Ptcd1^{+/+}$ littermates (Fig. 1B). Therefore, we analyzed the heterozygous mice for molecular and functional changes in their mitochondria compared to control littermate mice. We used northern blotting to investigate the steady-state levels of mt-RNAs from livers and hearts of $Ptcd1^{+/+}$ and $Ptcd1^{+/-}$ mice. The steady-state levels of the 12*S* rRNA were significantly increased in both the livers and hearts of $Ptcd1^{+/-}$ mice, as well as levels of specific unprocessed and mature mRNAs, such as *RNA19*, *mt-Nd5/Cytb*, *mt-Co1*, *mt-Co2*, *mt-Nd4l/4*, *mt-Nd5*, and *mt-Atp8/6* (Fig. 1C). The remaining levels of mature RNAs either showed an increased trend or were unaffected in the $Ptcd1^{+/-}$ mice compared to controls. Exceptions were the *mt-Nd6* and 16*S* rRNA that were significantly decreased in the $Ptcd1^{+/-}$ mice, indicating that the reduction in PTCD1 caused differential effects on mt-RNA metabolism. In addition, we found an overall increase in mt-tRNAs, specifically $tRNA^{Leu(UUR)}$, $tRNA^{Gln}$, $tRNA^{Trp}$, and $tRNA^{Glu}$ (Fig. 1C).

The effects of PTCD1 reduction in heart mitochondria of the $Ptcd1^{+/-}$ mice followed a similar trend to those found in liver mitochondria, but the magnitude of changes was less pronounced (Fig. 1D). In the heart, the 12*S* rRNA, *RNA19*, *mt-Co2*, *mt-Nd1*, *mt-Nd2*, and *mt-Nd4l/4* were also significantly increased, and most of the other tRNAs and mt-mRNAs showed an increased trend in the $Ptcd1^{+/-}$ mice compared to controls (Fig. 1D), as observed in the livers of heterozygous mice. These data indicate that haploinsufficiency of PTCD1 causes an increase in mt-RNA transcription and imbalanced mt-RNA metabolism.

In our previous work, we showed that PTCD1 affects mt-RNA processing in cells grown in high glucose, leading to accumulation of the *RNA19* that includes the 16*S* rRNA, $tRNA^{Leu(UUR)}$, and *mt-Nd1* region (*17*). Therefore, to investigate global effects of PTCD1 reduction in vivo across the entire mitochondrial transcriptome, we used an established RNA sequencing (RNA-Seq) method (*12*), where changes in rarer transcripts, such as precursors and partially processed transcripts, can be reliably identified at greater depth. Here, we applied the same method by making libraries from hearts and livers of three $Ptcd1^{+/+}$ and three $Ptcd1^{+/-}$ mice, where we captured longer reads across the entire mitochondrial transcriptome and excluded short RNAs, such as tRNAs, to analyze the sites most affected by PTCD1 reduction (figs. S2 and S3). We confirm the results from our northern blots that the mature mRNAs, as well as precursors such as the *RNA19* region, were increased in the $Ptcd1^{+/-}$ mice. The effects were more pronounced in the livers of these mice compared to hearts, despite the higher mt-RNA content in the heart, where it accounts for ~30% of total RNA (*24*). In addition, we observed increased accumulation of precursor transcripts that span specific tRNA coding regions (figs. S2 and S3). Upon closer inspection, we identified that the accumulation was particularly skewed toward the 3′ end in both heart and liver mitochondrial transcriptomes, suggesting that PTCD1 affects these processing sites preferentially. This is particularly evident in the regions spanning $tRNA^{Trp}$ and $tRNA^{Leu(UUR)}$ (Fig. 1, E and F). We used quantitative reverse transcription polymerase chain reaction (qRT-PCR) to validate the processing events across these junctions and confirmed that they were significantly enriched in the *Ptcd1* heterozygous mice compared to controls (Fig. 1G), further indicating that there is increased RNA transcription and accumulation of precursor transcripts as a consequence of PTCD1 reduction.

Reduction of PTCD1 decreases de novo protein synthesis of mitochondria-encoded proteins and the stability of large ribosomal proteins

Immunoblotting of mitochondrial proteins from livers and hearts of aged $Ptcd1^{+/+}$ and $Ptcd1^{+/-}$ mice showed that the heterozygous mice had ~50% lower levels of the PTCD1 protein compared to controls, indicating that haploinsufficiency underlies the molecular defects observed in these mice and this is consistent in liver and heart mitochondria (Fig. 2, A and B). Therefore, we investigated the effects of PTCD1 haploinsufficiency on mitochondrial- and nuclear-encoded OXPHOS polypeptides by immunoblotting in both liver (Fig. 2C) and heart mitochondria (Fig. 2D) and found no significant differences in their steady-state levels between the $Ptcd1^{+/+}$ and $Ptcd1^{+/-}$ mice, with the exception of cytochrome c oxidase subunit I (COXI), which was reduced in the livers of the heterozygous mice. Next, we analyzed the effects of PTCD1 reduction on mitochondrial proteins that regulate

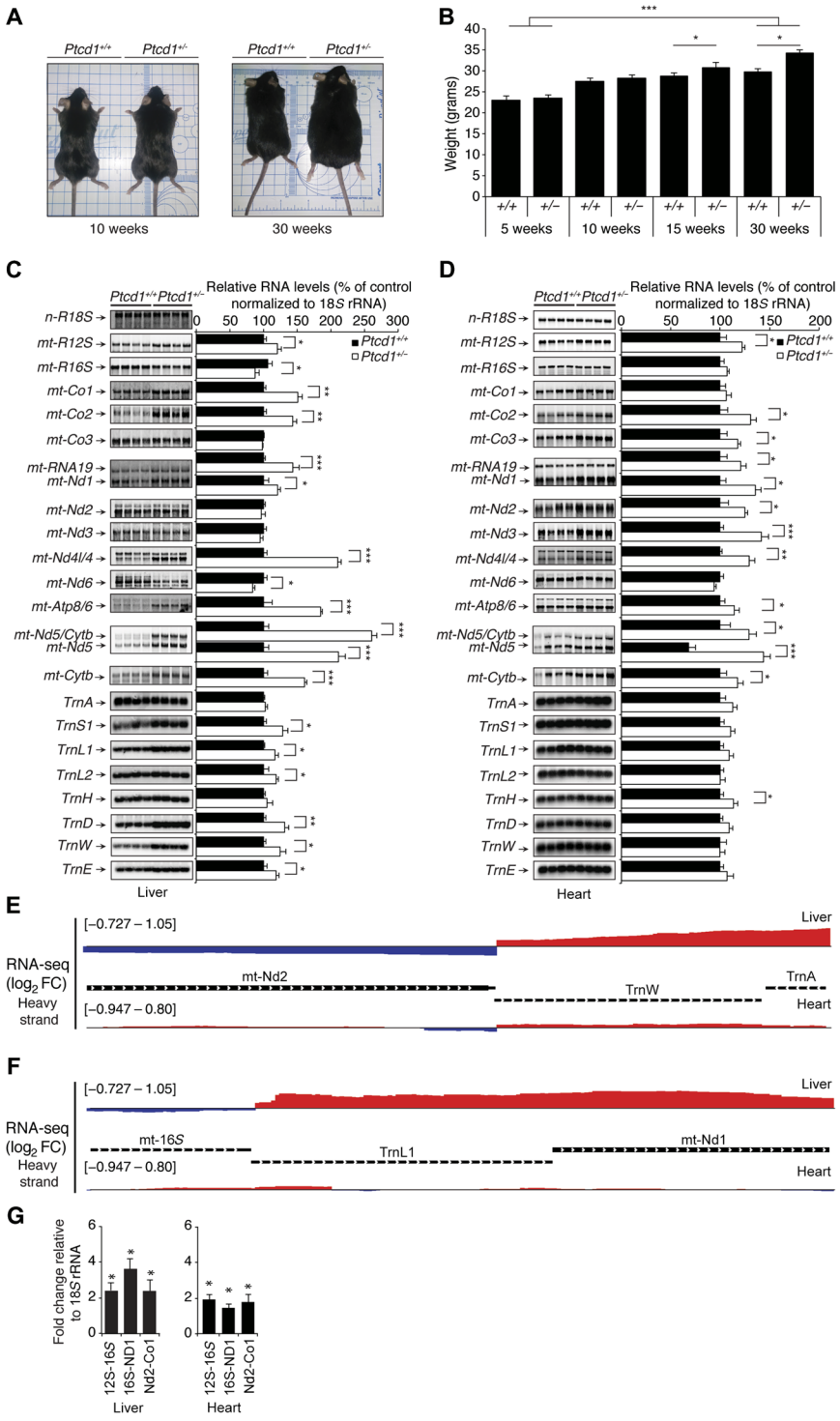

Fig. 1. Haploinsufficiency of *Ptcd1* affects mt-RNA metabolism. (**A**) Photographic representation of size and weight difference between control (*Ptcd1*$^{+/+}$) and heterozygote (*Ptcd1*$^{+/-}$) mice at 10 and 30 weeks of age. (**B**) Weight (in grams) of control (*Ptcd1*$^{+/+}$, $n = 6$) and heterozygote (*Ptcd1*$^{+/-}$, $n = 6$) mice at 5, 10, 15, and 30 weeks of age. Error bars indicate SEM. *$P < 0.05$, **$P < 0.01$, ***$P < 0.001$, Student's t test. The abundance of unprocessed and mature mitochondrial mRNAs, tRNAs, and rRNAs in livers (**C**) and hearts (**D**) of 30-week *Ptcd1*$^{+/+}$ and *Ptcd1*$^{+/-}$ mice were analyzed by northern blotting;18*S* rRNA was used as a loading control. The data are representative of results obtained from at least eight mice from each genotype and three independent biological experiments. (**E**) Genome browser view of the mean RNA-Seq coverage (log_2 fold change[KO_{mean}/$Ctrl_{mean}$]) in livers and hearts from three *Ptcd1*$^{+/+}$ and three *Ptcd1*$^{+/-}$ 30-week-old mice (mean normalized count) showing the region of mt-tRNA^{Trp} and the downstream effect on the 3′ end processing when PTCD1 is reduced. (**F**) Genome browser view of the mean RNA-Seq coverage (log_2 fold change[KO_{mean}/$Ctrl_{mean}$]) in livers and hearts from three *Ptcd1*$^{+/+}$ and three *Ptcd1*$^{+/-}$ 30-week-old mice (mean normalized count) showing the region of mt-tRNA$^{Leu(UUR)}$ and the downstream effect on the 3′ end processing when PTCD1 is reduced. (**G**) mt-RNA junctions were measured in total liver and heart RNA from *Ptcd1*$^{+/+}$ and *Ptcd1*$^{+/-}$ 30-week-old mice by qRT-PCR and normalized to 18*S* rRNA. Error bars indicate SEM. *$P < 0.05$, Student's t test.

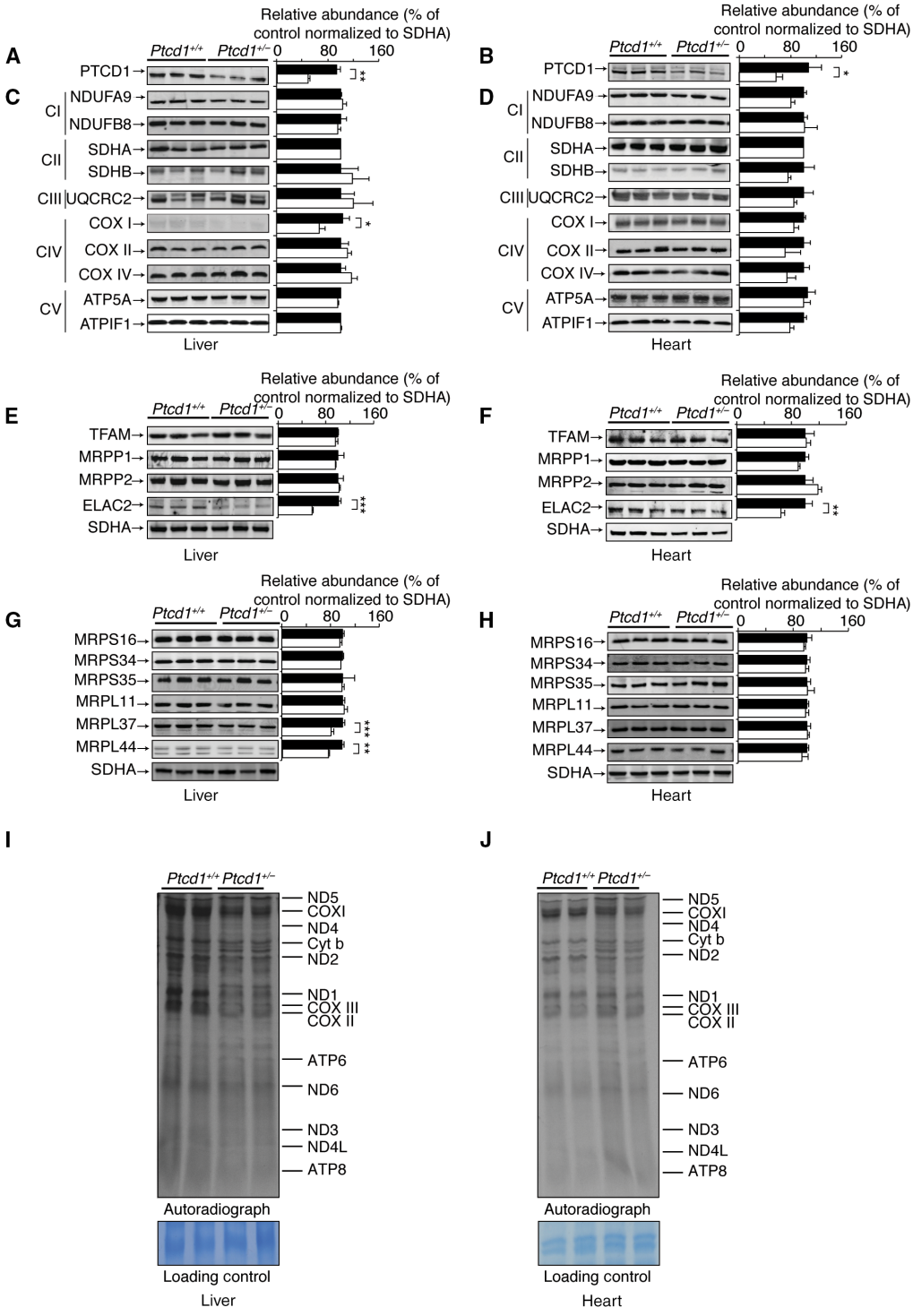

Fig. 2. PTCD1 reduction causes reduced mitochondrial protein synthesis. Mitochondrial proteins (25 μg) from liver and heart mitochondria from 30-week-old *Ptcd1*$^{+/+}$ and three *Ptcd1*$^{+/-}$ mice were resolved on 4 to 20% SDS-PAGE gels and immunoblotted against antibodies to investigate the steady-state levels of nuclear- and mitochondrial-encoded proteins. Succinate dehydrogenase complex subunit A (SDHA) was used as a loading control. PTCD1 levels are decreased by ~50% in liver (**A**) and heart (**B**) mitochondria, indicating its haploinsufficiency. Immunoblots of mitochondrial- and nuclear-encoded OXPHOS proteins in liver (**C**) and heart (**D**) mitochondria. Immunoblots of nuclear-encoded mtDNA- and RNA-binding proteins in liver (**E**) and heart (**F**) mitochondria. Immunoblots showing the levels of mitochondrial ribosomal proteins in liver (**G**) and heart (**H**) mitochondria. Relative abundance of proteins was measured using ImageJ software normalized to the loading control. Error bars indicate SEM. **P* < 0.05, ***P* < 0.01, ****P* < 0.001, Student's *t* test. The data are representative of results obtained from at least six mice from each genotype and three independent biological experiments. De novo protein synthesis in liver (**I**) and heart (**J**) from *Ptcd1*$^{+/+}$ and three *Ptcd1*$^{+/-}$ mice was measured by pulse incorporation of ^{35}S-labeled methionine and cysteine. Equal amounts of mitochondrial protein (50 μg) were separated by SDS-PAGE and visualized by autoradiography. Representative gels from three independent biological experiments are shown. All studies in this figure were performed in 30-week-old mice.

gene expression and RNA processing (Fig. 2, E and F). Although there were no differences in the levels of TFAM and the RNase P proteins MRPP1 and MRPP2, we found a significant reduction in the levels of the mitochondrial RNase Z enzyme (ELAC2), which is responsible for cleavage of tRNAs at their 3′ ends, in liver and heart mitochondria from *Ptcd1*$^{+/-}$ mice compared to controls (Fig. 2, E and F). This further implicates PTCD1 in RNA maturation within mitochondria.

We have shown previously that impaired mt-RNA processing can affect the stability of mitochondrial ribosomal proteins (*12*, *17*); therefore, we investigated whether decrease in PTCD1 affects their stability. Immunoblotting revealed that only the levels of the large ribosomal subunit proteins MRPL37 and MRPL44 were reduced significantly in the liver mitochondria from *Ptcd1*$^{+/-}$ mice, but not in the small ribosomal subunit proteins MRPS16, MRPS34, and MRPS35 that were analyzed (Fig. 2G). The levels of the mitoribosomal proteins from both the small and large subunits were not different in heart mitochondria from *Ptcd1*$^{+/+}$ and *Ptcd1*$^{+/-}$ mice (Fig. 2H), indicating that mitochondrial ribosomal proteins in the liver are more affected by the reduction of PTCD1 compared to the heart.

Next, we investigated mitochondrial protein synthesis by de novo labeling to determine whether reduction in PTCD1 affects the rate of translation of the newly produced polypeptides. We found decreased translation of most polypeptides in liver mitochondria from *Ptcd1*$^{+/-}$ mice (Fig. 2I). The effects on protein synthesis in heart mitochondria from *Ptcd1*$^{+/-}$ mice were subtle, albeit consistent with the more modest changes observed in heart mitochondria by immunoblotting and northern blotting (Fig. 2J). In older, 40-week-old mice, we observed decreased protein synthesis in both liver and heart mitochondria from *Ptcd1*$^{+/-}$ mice (fig. S4, A and B), indicating that the molecular changes in the heart are more apparent with age, reflecting the higher mt-RNA content in the heart (*24*). These changes are consistent at the steady-state protein level, where immunoblotting for the OXPHOS complexes and the mitochondrially encoded COXII and COXIII subunits show significant decreases in both liver and heart mitochondria from 40-week-old *Ptcd1*$^{+/-}$ mice (fig. S4, C and D), although the effects are still more pronounced in the liver, suggesting that the liver is more affected by the reduction of PTCD1 compared to the heart. We conclude that despite the increased levels of mature mt-RNAs, the allelic loss of PTCD1 results in decreased de novo translation, suggesting that increased transcription may be a compensatory response to decreased protein synthesis.

PTCD1 is important for mitochondrial respiratory complex biogenesis and function

We measured oxygen consumption in liver and heart mitochondria to determine whether mitochondrial respiratory function was affected when PTCD1 levels were reduced. Mitochondrial state 3 and state 4 respiration using glutamate/malate or succinate as the substrates were significantly decreased in the liver (Fig. 3A) but not heart (Fig. 3B) mitochondria from 30-week-old *Ptcd1*$^{+/-}$ mice. Similarly, the maximum capacity of the respiratory chain, which was measured in the presence of the uncoupler carbonyl cyanide *p*-trifluoromethoxyphenylhydrazone (FCCP), was also significantly decreased in liver mitochondria from *Ptcd1*$^{+/-}$ mice compared to controls (Fig. 3A). We also investigated the effects of PTCD1 reduction on mitochondrial respiration in 40-week-old mice and show that in these older mice OXPHOS function is decreased in both the livers and hearts of *Ptcd1*$^{+/-}$ mice compared to controls (fig. S4, E and F). The effects of PTCD1 reduction on OXPHOS capacity are more apparent with aging, as 10-week-old mice have normal OXPHOS function (fig. S5, A and B). These findings indicate that mitochondrial function in the liver is affected before the heart, further indicating that the excess mt-RNA in the heart may compensate and protect its function when mitochondrial gene expression is compromised.

Because mitochondrial respiration was affected in the *Ptcd1*$^{+/-}$ mice, we analyzed the levels of the mitochondrial respiratory complexes by blue native polyacrylamide gel electrophoresis (BN-PAGE). We observed a noticeable reduction of the respiratory complex V in the liver of *Ptcd1*$^{+/-}$ mice compared to controls, and a slight decrease in complexes I and III, but very mild changes in *Ptcd1*$^{+/-}$ heart mitochondria (Fig. 3, C and D). We further quantified the changes following BN-PAGE and immunoblotting of each complex to confirm that the levels of complex V were significantly reduced by ~20% in liver mitochondria from *Ptcd1*$^{+/-}$ mice compared to controls, and there was a slight decrease in complex III (Fig. 3C); however, the levels of respiratory complexes were not significantly changed in heart mitochondria between heterozygote and wild-type mice (Fig. 3D). To investigate the assembly and activity of complex V, the adenosine triphosphate (ATP) synthase, we used BN-PAGE followed by in-gel activity staining (Fig. 3, E and F). There was a noticeable reduction in adenosine triphosphatase activity, a decrease in the monomeric form of the ATP synthase, and significant reduction in the dimer and F1 subcomplexes of the ATP synthase in liver mitochondria from the *Ptcd1*$^{+/-}$ mice compared to controls (Fig. 3E). In contrast, there were no differences in the activity or levels of the ATP synthase in heart mitochondria from the *Ptcd1*$^{+/+}$ and *Ptcd1*$^{+/-}$ mice (Fig. 3F). These findings are consistent with our measurements of the ATP/ADP (adenosine diphosphate) ratio for both young and adult *Ptcd1*$^{+/+}$ and *Ptcd1*$^{+/-}$ mice (fig. S4, E and H), where we observe a significant decrease of ~50% of ATP levels in the livers from old *Ptcd1*$^{+/-}$ mice (fig. S4G), consistent with decreased OXPHOS function and mitochondrial uncoupling and reduced complex V activity and levels. Our findings indicate that haploinsufficiency of PTCD1 and decreased protein synthesis in mitochondria can have tissue-specific downstream consequences on the stability and function of the OXPHOS system.

Heterozygous *Ptcd1* mice have remodeled cristae and altered mitochondrial morphology

The dynamin-like guanosine triphosphatase OPA1 mediates mitochondrial fusion and fission and regulates mitochondrial cristae morphology (*25*). The processing of OPA1 by the OMA-1 and YME1L peptidases is crucial for normal mitochondrial morphology by balancing the distribution of the long isoforms of OPA1 (L-OPA1) and short isoforms of OPA1 (S-OPA1) that are important to maintain fusion and fission, respectively [reviewed by MacVicar and Langer (*26*)]. Recently, OPA1 and cristae remodeling have been implicated in the assembly and stability of the respiratory complexes as well as their function (*27*, *28*). Because we found that mitochondria of the *Ptcd1*$^{+/-}$ mice were mildly uncoupled and that this uncoupling affected the respiratory complexes, we investigated whether the processing of OPA1 and its processing peptidase OMA-1 was also affected. In liver mitochondria from *Ptcd1*$^{+/-}$ mice, we found decreased L-OPA1 levels and markedly increased S-OPA1 abundance (Fig. 3G), whereas the levels of the short and long isoforms of OPA1 were not changed between heart mitochondria from *Ptcd1*$^{+/+}$ and *Ptcd1*$^{+/-}$ mice (Fig. 3H). Furthermore, the metalloproteinase OMA-1 is increased in liver mitochondria from *Ptcd1*$^{+/-}$ mice but not in heart mitochondria from these mice compared to their respective controls (Fig. 3, G and H). The mitochondrial membrane potential was decreased in liver mitochondria from *Ptcd1*$^{+/-}$ 30-week-old mice

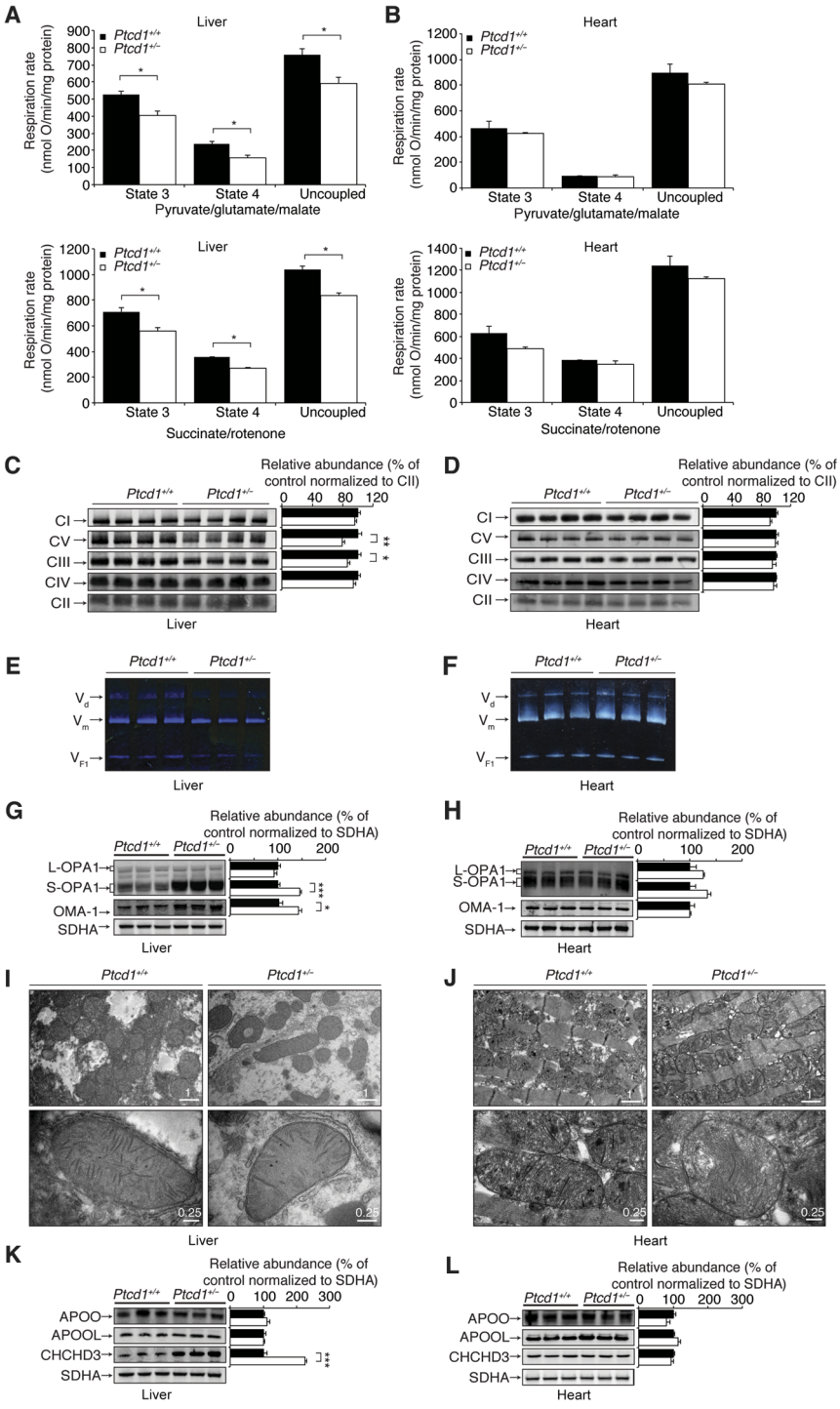

Fig. 3. Reduction of PTCD1 affects the biogenesis of the respiratory chain, causing mild uncoupling and changes in mitochondrial morphology. Phosphorylating (state 3) and uncoupled respiration in the presence of up to 3 μM FCCP was measured in liver (**A**) and heart (**B**) mitochondria from four 30-week-old *Ptcd1*$^{+/+}$ and four *Ptcd1*$^{+/−}$ mice using an OROBOROS oxygen electrode using either pyruvate, glutamate, and malate or succinate as substrates in the presence of inhibitors. Isolated liver (**C**) and heart (**D**) mitochondria (75 μg) from 30-week-old mice were treated with 1% *n*-dodecyl-β-D-maltoside and resolved on 4 to 16% BN-PAGE gel. Immunoblotting with the blue native OXPHOS cocktail antibody was used to visualize respiratory complexes. Error bars indicate SEM. **P* < 0.05, ***P* < 0.01, Student's *t* test. In-gel activity stains were used for complex V in liver (**E**) and heart (**F**) mitochondria. Steady-state levels of OPA1 and OMA-1 in liver (**G**) and heart (**H**) mitochondria from at least eight *Ptcd1*$^{+/+}$ and eight *Ptcd1*$^{+/−}$ mice were measured by immunoblotting using SDHA as a loading control. Error bars indicate SEM. ***P* < 0.01, ****P* < 0.001, Student's *t* test. Mitochondrial morphology and cristae structure in *Ptcd1*$^{+/+}$ and four *Ptcd1*$^{+/−}$ livers (**I**) and hearts (**J**) were determined using TEM. The data are representative of results obtained from at least three mice from each genotype. Scale bars, 0.25 μm (bottom panels) and 1 μm (top panels). The abundance of MICOS complex proteins was measured in liver (**K**) and heart (**L**) mitochondria from at least eight *Ptcd1*$^{+/+}$ and eight *Ptcd1*$^{+/−}$ mice using immunoblotting. SDHA was used as a loading control. Error bars indicate SEM. ****P* < 0.001, Student's *t* test.

compared to controls and in mouse embryonic fibroblasts (MEFs) from *Ptcd1*$^{+/-}$ mice compared to controls (fig. S6, A and B), consistent with the respiration measurements. Furthermore, we observed a more fragmented appearance of mitochondria in the *Ptcd1*$^{+/-}$ MEFs compared to controls, particularly when they were grown in low glucose or galactose (fig. S6C).

Transmission electron microscopy (TEM) was used to investigate how decreased membrane potential and increased levels of S-OPA1 affect mitochondrial morphology in livers compared to hearts from *Ptcd1*$^{+/-}$ mice and their respective controls from *Ptcd1*$^{+/+}$ mice (Fig. 3, I and J). In the livers of *Ptcd1*$^{+/-}$ mice, we observed mitochondria with fewer cristae compared to control mice (Fig. 3I). In the hearts of *Ptcd1*$^{+/-}$ mice, the morphology of mitochondria was less affected than in the liver, although there was a higher number of surrounding smaller mitochondria and the muscle fibers had less dense z lines (Fig. 3J). Most of the heart mitochondria had hollow parts that lacked cristae, although this was not as apparent as in the livers of *Ptcd1*$^{+/-}$ mice (Fig. 3, I and J, lower panels).

Because we observed morphological changes in mitochondria and their cristae, we next analyzed whether the abundance of the mitochondrial contact site and cristae organizing system (MICOS) components was affected in the *Ptcd1*$^{+/-}$ mice compared to controls (Fig. 3, K and L). We immunoblotted for MICOS components that were associated with the inner membrane, such as APOO and APOOL, because we have found PTCD1 localized in the matrix as well as the inner mitochondrial membrane (*16*). The levels of these proteins were not changed in liver or heart mitochondria between *Ptcd1*$^{+/+}$ and *Ptcd1*$^{+/-}$ mice. However, the level of the MICOS protein CHCHD3, previously identified to interact with OPA1 (*29*), was increased significantly in liver mitochondria from the *Ptcd1*$^{+/-}$ mice compared to controls (Fig. 3K) or heart mitochondria from both genotypes (Fig. 3L). Together, these data indicate that mild uncoupling of mitochondria affects their morphology and cristae as well as the MICOS components closely associated with OPA1 and shift the balance of the short and long isoform of OPA1. Haploinsufficiency of PTCD1 over time cannot be compensated by an increase in CHCHD3 in an attempt to overcome morphological changes induced by uncoupling and accumulation of S-OPA1.

Adult-onset heart hypertrophy and liver steatosis in heterozygous *Ptcd1*$^{+/-}$ mice

Previously, we found that complete knockout of the endonuclease component of the mitochondrial RNase P complex, MRPP3, responsible for 5′ end tRNA processing, in the heart resulted in a severe cardiomyopathy followed by premature death at 11 weeks (*12*). Although the *Ptcd1*$^{+/-}$ mice do not die at such an early age, the haploinsufficiency of PTCD1 alone causes defects in RNA metabolism/protein synthesis that are sufficient with age to cause mitochondrial dysfunction and significant weight gain (Fig. 1A). Therefore, we analyzed liver and heart function of *Ptcd1*$^{+/-}$ mice compared to *Ptcd1*$^{+/+}$ mice to investigate how decreased protein synthesis, OXPHOS uncoupling, and altered mitochondrial morphology can exacerbate dysfunction and lead to pathology. Oil red O staining of liver sections revealed extensive accumulation of small lipid droplets in the *Ptcd1*$^{+/-}$ mice, causing pronounced fibrosis with age (Fig. 4, A and B). The livers of the adult *Ptcd1*$^{+/-}$ mice are chronically injured, with a greater number of oval-shaped liver progenitor cells observed (Fig. 4A). Hematoxylin and eosin (H&E) staining of the liver further confirms that binucleated hepatocytes represent the major dividing cell type in the regenerating liver of *Ptcd1*$^{+/-}$ mice compared to controls (Fig. 4B). We also observed an

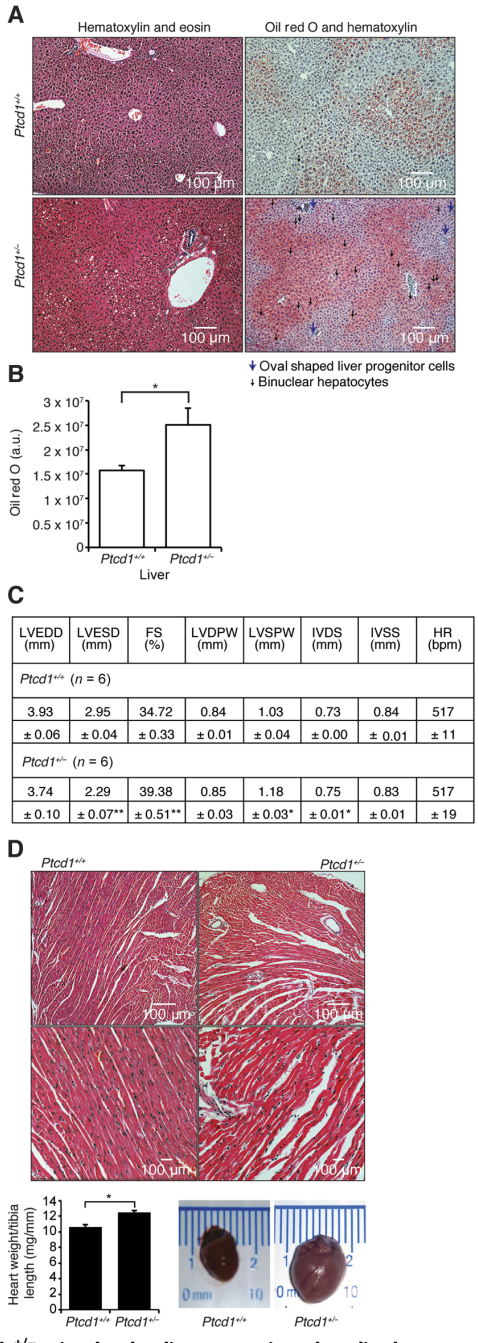

LVEDD (mm)	LVESD (mm)	FS (%)	LVDPW (mm)	LVSPW (mm)	IVDS (mm)	IVSS (mm)	HR (bpm)
Ptcd1$^{+/+}$ (n = 6)							
3.93	2.95	34.72	0.84	1.03	0.73	0.84	517
± 0.06	± 0.04	± 0.33	± 0.01	± 0.04	± 0.00	± 0.01	± 11
Ptcd1$^{+/-}$ (n = 6)							
3.74	2.29	39.38	0.85	1.18	0.75	0.83	517
± 0.10	± 0.07**	± 0.51**	± 0.03	± 0.03*	± 0.01*	± 0.01	± 19

Fig. 4. *Ptcd1*$^{+/-}$ mice develop liver steatosis and cardiac hypertrophy. (**A**) Liver sections cut to 5- or 10-μm thickness were stained with H&E or Oil red O and hematoxylin, respectively, from 30-week-old *Ptcd1*$^{+/+}$ (n = 6) and *Ptcd1*$^{+/-}$ (n = 6) mice. (**B**) Quantitative measurement of Oil red O staining using ImageJ. Values are means ± SEM. *P < 0.05, Student's t test. (**C**) ECG parameters for *Ptcd1*$^{+/+}$ (n = 5) and *Ptcd1*$^{+/-}$ (n = 5) 40-week-old mice. LVEDD, left ventricular end diastolic diameter; LVESD, left ventricular end systolic diameter; FS, fractional shortening; LVDPW, left ventricular posterior wall in diastole; LVSPW, left ventricular posterior wall in systole; IVDS, intraventricular septum in diastole; IVSS, intraventricular septum in systole; HR, heart rate. Values are means ± SEM. *P < 0.05 compared with *Ptcd1*$^{+/+}$, **P < 0.01, Student's t test. (**D**) Heart sections cut to 5-μm thickness were stained with H&E from aged *Ptcd1*$^{+/+}$ (n = 6) and *Ptcd1*$^{+/-}$ (n = 6) mice. Scale bars, 100 μm. Enlarged hearts were determined as a measure of heart weight relative to tibia length; *P < 0.05 compared with *Ptcd1*$^{+/+}$, Student's t test. Photographic representation of size difference between *Ptcd1*$^{+/+}$ and *Ptcd1*$^{+/-}$ hearts in adult mice.

increase in the number of hepatic blood vessels, which may be a compensatory effect in an effort to increase blood flow to the damaged liver. Together, these results indicate that *Ptcd1*$^{+/-}$ mice have hepatic steatosis.

Impaired 3′ end tRNA processing has been shown to cause cardiomyopathy in patients with mutations in ELAC2 (*30*); therefore, echocardiography (ECG) was performed on the aged *Ptcd1*$^{+/-}$ and *Ptcd1*$^{+/+}$ mice. *Ptcd1*$^{+/-}$ mice had altered cardiac function consistent with the development of cardiac hypertrophy, including a significant increase in the left ventricular posterior wall in systole and intraventricular septum in diastole (thicker walls), a significant decrease in the left ventricular end systolic diameter (narrowing chamber), and an increase in fractional shortening, which demonstrates a hypercontractile heart (Fig. 4C). H&E staining of the aged hearts of *Ptcd1*$^{+/-}$ mice revealed enlarged nuclei, which are more sparsely dispersed within the heart tissue and consistent with the enlarged size of the hearts, indicative of hypertrophy in the heart (Fig. 4D). These results suggest that a reduction of PTCD1 has pathological consequences for both the liver and heart with aging, although more severe molecular changes are identified in the livers of heterozygous mice.

Adult-onset obesity in *Ptcd1*$^{+/-}$ mice leads to glucose intolerance and insulin resistance

To investigate the metabolic consequences of PTCD1 haploinsufficiency, we monitored the weight of *Ptcd1*$^{+/+}$ and *Ptcd1*$^{+/-}$ mice from 5 to 30 weeks of age. During this time, we kept a record of their weight gain and food intake, by measuring the input and output of food each week. *Ptcd1*$^{+/-}$ mice did not display different eating habits, appetites, or intake of food relative to *Ptcd1*$^{+/+}$ mice between the ages of 5 and 30 weeks. Between the ages of 5 and 15 weeks, there was no significant difference in weight between *Ptcd1*$^{+/-}$ mice and their wild-type littermates (Fig. 5A). From 15 weeks, the *Ptcd1*$^{+/-}$ mice were starting to show a significant increase in weight compared to controls, and by 30 weeks of age, *Ptcd1*$^{+/-}$ mice were significantly heavier, by approximately 5 g, compared to *Ptcd1*$^{+/+}$ mice (Fig. 5A). Measurement of intra-abdominal epididymal pad weights showed greater visceral lipid deposition in adult *Ptcd1*$^{+/-}$ mice than *Ptcd1*$^{+/+}$ mice, no differences in lipid deposition between *Ptcd1*$^{+/-}$ and *Ptcd1*$^{+/+}$ 10-week-old mice (Fig. 5B).

Glucose tolerance testing (GTT) of *Ptcd1*$^{+/+}$ and *Ptcd1*$^{+/-}$ mice fed a normal chow diet (NCD) showed that the *Ptcd1*$^{+/-}$ mice were glucose-intolerant at 15 and 30 weeks of age (Fig. 5, C and D). Insulin tolerance testing (ITT) revealed that early in life, at 11 weeks, the *Ptcd1*$^{+/-}$ mice are slightly insulin-sensitive; however, by 16 weeks of age, there was no difference in insulin sensitivity between *Ptcd1*$^{+/+}$ and *Ptcd1*$^{+/-}$ mice (Fig. 5E). Subsequently, by 30 weeks of age, the *Ptcd1*$^{+/-}$ mice had developed insulin resistance compared to their wild-type counterparts (Fig. 5, E and F), consistent with their weight gain and glucose intolerance at this age. This shows that, with age, *Ptcd1*$^{+/-}$ mice have decreased glucose tolerance and increased insulin resistance compared to their control littermates, indicating that decreased protein synthesis with age impairs mitochondrial function and membrane morphology that leads to a metabolic switch, causing weight gain and consequent metabolic desensitization to insulin.

Reduction of PTCD1 causes early-onset hormonal changes that contribute to the development of disease in response to mitochondrial dysfunction

Alterations in the levels of cholesterol and triglycerides, insulin, leptin, interleukin-6 (IL-6), and fibroblast growth factor 21 (FGF-21) have all been linked to the development of obesity and metabolic syndrome (*31*). Therefore, we investigated the levels of hormones and growth factors involved in glucose and lipid metabolism, and the regulation of food intake and energy expenditure by enzyme-linked immunosorbent assays (ELISAs) in serum isolated from 10- to 30-week-old *Ptcd1*$^{+/-}$ and *Ptcd1*$^{+/+}$ mice fed an NCD. In 10-week-old mice, the levels of insulin, triglycerides, cholesterol, and IL-6 were not statistically different between the *Ptcd1*$^{+/+}$ and *Ptcd1*$^{+/-}$ mice, whereas leptin and FGF-21 were both significantly elevated in the *Ptcd1*$^{+/-}$ mice (Fig. 6A). In contrast, we found significantly increased levels of triglycerides, IL-6, leptin, and FGF-21 in the 30-week-old *Ptcd1*$^{+/-}$ mice compared to the *Ptcd1*$^{+/+}$ mice (Fig. 6B). The increases in triglycerides and leptin are consistent with significant weight gain, and the elevated FGF-21 is consistent with cardiac dysfunction, as has been observed previously in other models of heart disease, which has led to its use as a marker of mitochondrial dysfunction (*32*, *33*). Increased IL-6 levels are consistent with liver injury in the *Ptcd1*$^{+/-}$ mice involving mitochondrial dysfunction and metabolic syndrome. Increases in phosphorylation of stress-activated protein kinase (SAPK)/c-Jun N-terminal kinase (JNK), in response to profoundly elevated IL-6, were identified in the livers of 10- and 30-week-old *Ptcd1*$^{+/-}$ mice compared to *Ptcd1*$^{+/+}$ mice (Fig. 6C). Similarly, increased SAPK/JNK phosphorylation was found in the hearts of 10- and 30-week-old *Ptcd1*$^{+/-}$ mice compared to controls (Fig. 6D), indicating activation of inflammatory signaling pathways in the development of both hepatic steatosis and cardiac hypertrophy.

Tissue-specific regulation of the mTOR pathway in response to the severity of mitochondrial dysfunction

Severe mitochondrial dysfunction has been shown to stimulate up-regulation of the mTOR pathway via the mTOR complex 1 (mTORC1), to increase cytosolic protein synthesis as a compensatory measure in an effort to overcome OXPHOS defects (*34*–*36*). Therefore, we investigated these pathways to determine how mitochondrial dysfunction may cause retrograde changes in these cell signaling pathways. Immunoblotting revealed that Akt phosphorylation is significantly increased in the livers of *Ptcd1*$^{+/-}$ mice compared to *Ptcd1*$^{+/+}$ mice (Fig. 7A) and relative to the steady-state levels of Akt. Next, we investigated the mTOR signaling pathway in the livers of *Ptcd1*$^{+/-}$ mice and found that both the steady-state and phosphorylated levels of mTOR are significantly decreased compared to controls (Fig. 7A). Because the formation of mTORC1 and mTORC2 differs by the association of mTOR with either Raptor or Rictor, respectively [reviewed by Johnson *et al.* (*36*)], we analyzed the effects on both of these proteins. We found that in the livers of *Ptcd1*$^{+/-}$ mice, the levels of Rictor, but not Raptor, are significantly decreased compared to those in control mice (Fig. 7A). Analyses of the downstream substrates of the mTORC1 pathway, the ribosomal protein S6 and translational initiator, 4E-BP1, in livers, revealed that there were no significant changes in their steady-state levels or their phosphorylation status (Fig. 7A). Changes in mitochondrial ATP/ADP levels are sensed by the phosphorylation of the AMPKα, and increase in AMPKα phosphorylation represses mTORC1 signaling (*36*). In the livers of *Ptcd1*$^{+/-}$ mice, we found increased phosphorylation of AMPKα (Fig. 7B), consistent with decreased ATP levels (fig. S4G) and decreased mTOR phosphorylation (Fig. 7A) compared to controls. Together, these data suggest that Akt phosphorylation in the livers of *Ptcd1*$^{+/-}$ mice acts via the mTORC2 pathway.

Although we found increased phosphorylation of Akt in both heart and liver tissue of *Ptcd1*$^{+/-}$ mice compared to *Ptcd1*$^{+/+}$ controls, we identified increased phosphorylation of mTOR and its substrates S6 and 4E-BP1 only in heart tissue of *Ptcd1*$^{+/-}$ mice (Fig. 7C). Here,

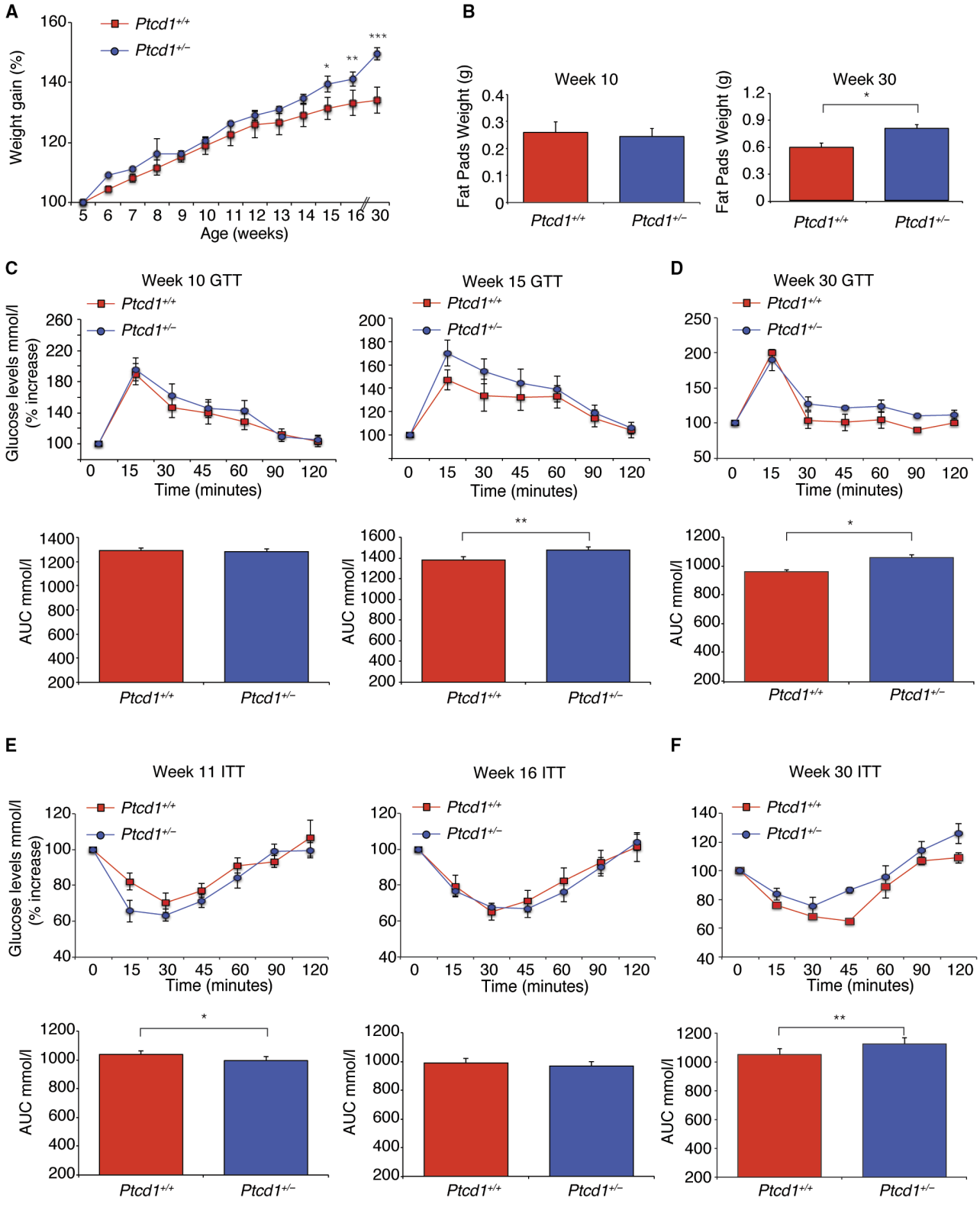

Fig. 5. Reduction of PTCD1 causes adult-onset obesity and insulin resistance. (**A**) Percentage increase of weight gain from 5 to 30 weeks of age between *Ptcd1*$^{+/+}$ ($n = 12$) and *Ptcd1*$^{+/-}$ ($n = 12$) mice. *$P < 0.05$, **$P < 0.01$, ***$P < 0.001$, Student's *t* test. (**B**) Weight of intra-abdominal epididymal fat pads in grams for young and adult *Ptcd1*$^{+/+}$ ($n = 4$) and *Ptcd1*$^{+/-}$ ($n = 4$) mice. (**C**) Glucose tolerance in 10- and 15-week-old *Ptcd1*$^{+/+}$ ($n = 12$) and *Ptcd1*$^{+/-}$ ($n = 12$) mice (young mice). (**D**) Glucose tolerance in 30-week-old *Ptcd1*$^{+/+}$ ($n = 12$) and *Ptcd1*$^{+/-}$ ($n = 12$) mice (aged mice). (**E**) Insulin sensitivity in 11- and 16-week-old *Ptcd1*$^{+/+}$ ($n = 12$) and *Ptcd1*$^{+/-}$ ($n = 12$) mice (young mice). Quantitative values are the area under the curve (AUC) ± SEM. *$P < 0.05$, Student's *t* test. (**F**) Insulin sensitivity in 30-week-old *Ptcd1*$^{+/+}$ ($n = 12$) and *Ptcd1*$^{+/-}$ ($n = 12$) mice. Quantitative values are the AUC ± SEM. **$P < 0.01$, Student's *t* test.

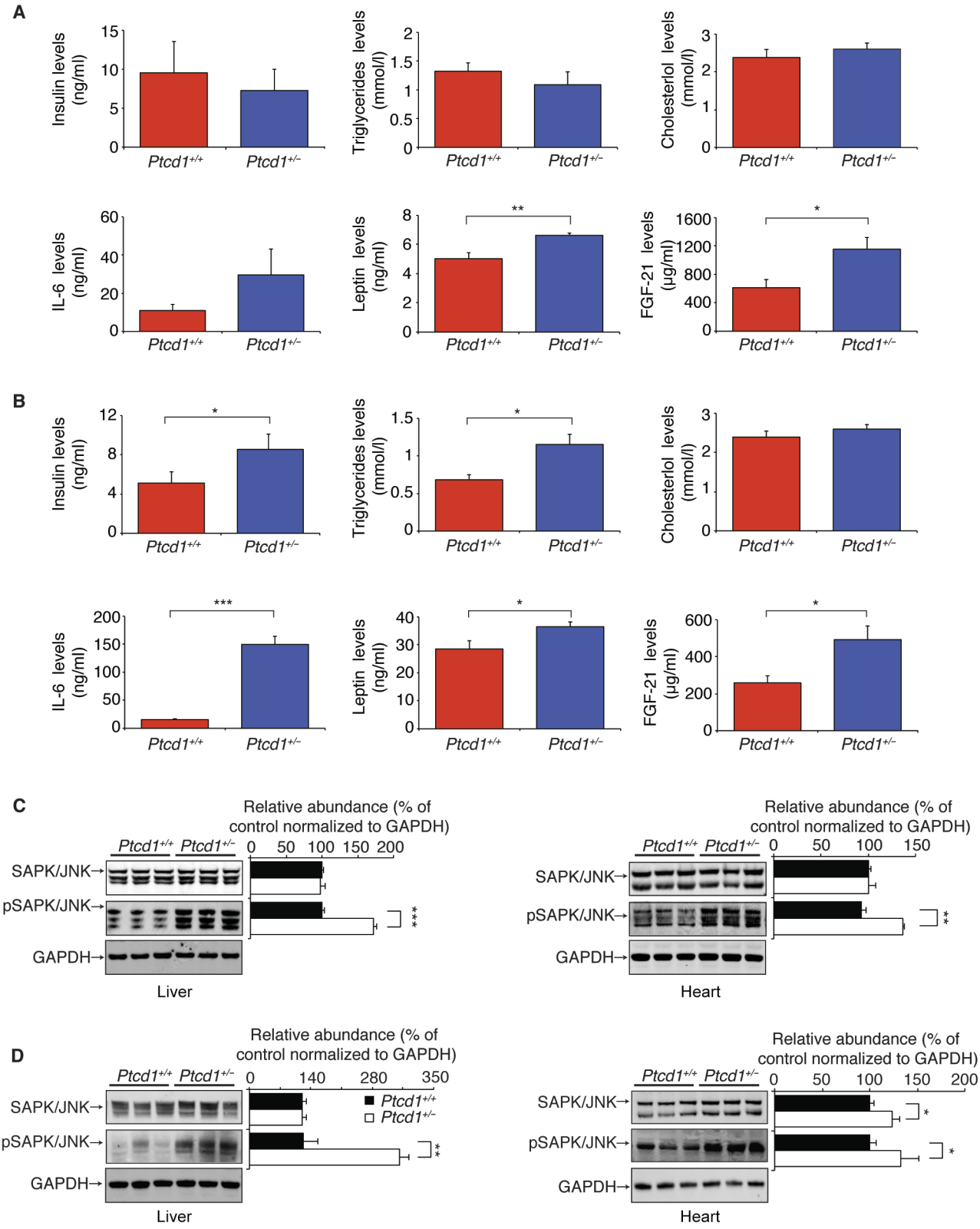

Fig. 6. Metabolic hormones, growth factors, and proinflammatory cytokines increase with age in the *Ptcd1*$^{+/-}$ mice. (**A**) Insulin, triglycerides, cholesterol, IL-6, leptin, and FGF-21 levels were measured in serum obtained from 10-week-old *Ptcd1*$^{+/+}$ ($n = 6$) and *Ptcd1*$^{+/-}$ ($n = 6$) mice. (**B**) Insulin, triglycerides, cholesterol, IL-6, leptin, and FGF-21 levels were measured in serum obtained from 30-week-old *Ptcd1*$^{+/+}$ ($n = 6$) and *Ptcd1*$^{+/-}$ ($n = 6$) mice. Endogenous levels of the SAPK/JNK and its phosphorylated form (Thr^{183}/Tyr^{185}) were determined by immunoblotting of whole liver and heart lysates from 10-week-old (**C**) or 30-week-old (**D**) *Ptcd1*$^{+/+}$ and *Ptcd1*$^{+/-}$ mice. GAPDH (glyceraldehyde-3-phosphate dehydrogenase) was used as a loading control. Error bars indicate SEM. *$P < 0.05$, **$P < 0.01$, ***$P < 0.001$, Student's *t* test.

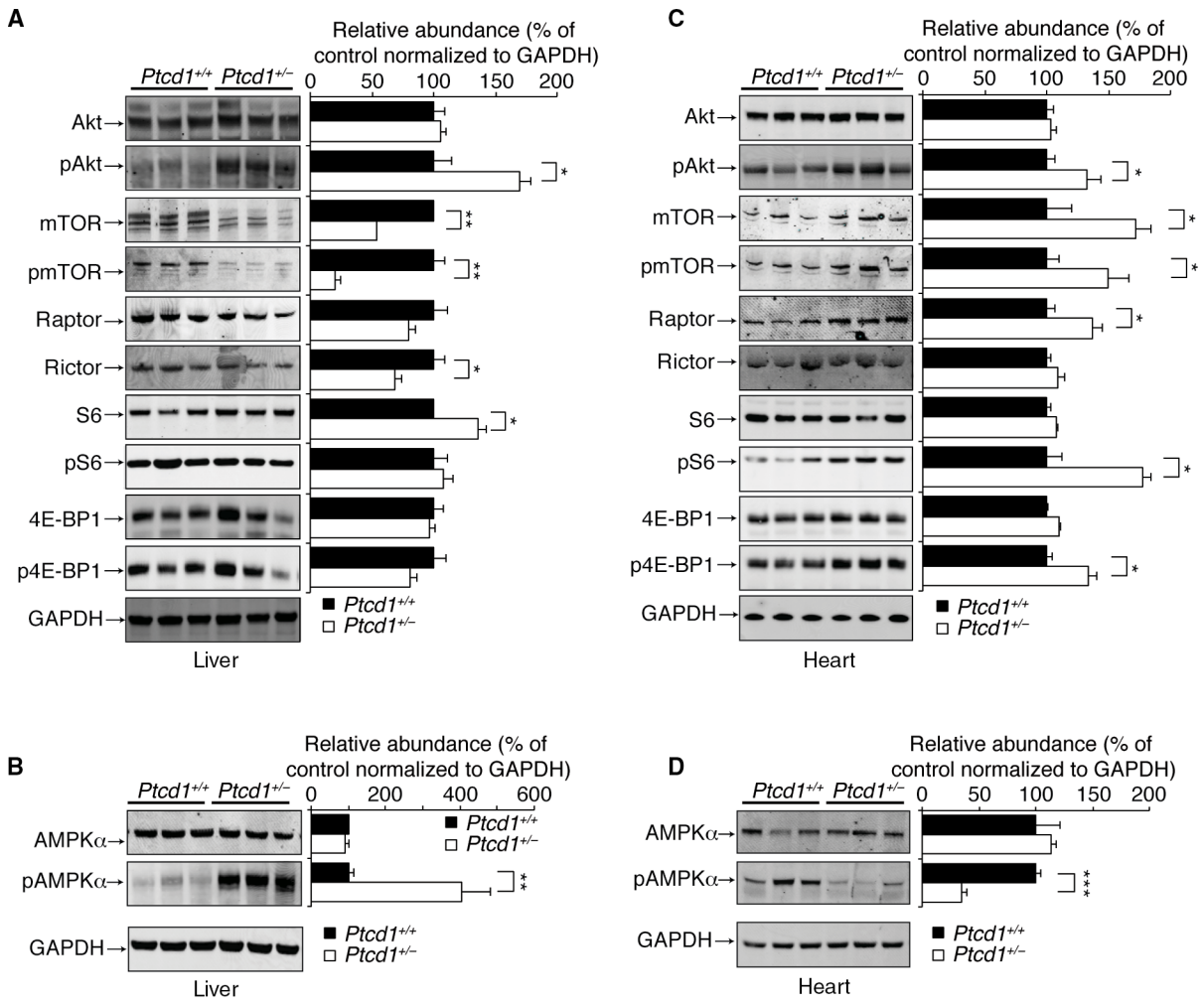

Fig. 7. The mTOR signaling pathway is differentially regulated in response to mitochondrial dysfunction in *Ptcd1*$^{+/-}$ mice. The mTOR pathway was assessed by immunoblotting using specific antibodies upstream and downstream of mTOR in liver (**A**) and heart (**C**) lysates from *Ptcd1*$^{+/+}$ and *Ptcd1*$^{+/-}$ 30-week-old mice using GAPDH as a loading control. Immunoblotting was used to measure the abundance of the phosphorylated (Thr^{172}) and nonphosphorylated form of AMPKα in liver (**B**) and heart (**D**) lysates from 30-week-old *Ptcd1*$^{+/+}$ and *Ptcd1*$^{+/-}$ mice using GAPDH as a loading control. Relative abundance of proteins was measured using ImageJ software normalized to the loading control. Error bars indicate SEM. *$P < 0.05$, **$P < 0.01$, ***$P < 0.001$, Student's *t* test. The data are representative of results obtained from at least six mice from each genotype and three independent biological experiments.

we also found that levels of Raptor are increased in the heterozygote hearts, whereas the levels of Rictor are not different between the heterozygote and control mice (Fig. 7C). The increase in mTOR signaling is consistent with the decreased phosphorylation status of AMPKα in the hearts of *Ptcd1*$^{+/-}$ mice compared to controls (Fig. 7D). These opposing effects in the heart compared to the liver indicate that the mTORC1 signaling is activated in the hearts of PTCD1 heterozygote mice, confirming differential mTOR regulation in response to mitochondrial dysfunction between highly proliferative tissues, such as the liver, and postmitotic tissue, such as the heart.

DISCUSSION

mt-RBPs are key to mammalian mitochondrial gene expression and biogenesis, by regulating transcription, RNA processing, RNA maturation, stability, and translation (*1*, *2*). This is evident from mutations in nuclear genes encoding different mt-RBPs, including LRPPRC, ELAC2, MRPP1, and TACO1, that cause mitochondrial dysfunction, disease, and frequently death in humans (*30*, *37*–*39*). Furthermore, mouse models, where mt-RBPs have been knocked out, show that they are essential for embryo development and survival (*10*, *12*, *13*, *21*, *23*). Here, we show that PTCD1 is essential for life and that even haploinsufficiency of this protein leads to mitochondrial dysfunction, metabolic defects, and disease, which has not been observed before for an mt-RBP. Reduction of PTCD1 has a significant impact on mt-RNA metabolism in vivo particularly because decrease in PTCD1 also affects the levels of the mitochondrial RNase Z but not RNase P, validating our previous identified association of PTCD1 with ELAC2 (*17*). Despite processing defects, we observed an increase in most mature mt-RNAs, likely as a result of increased transcription, previously observed in models where RNA processing and stability are affected (*12*, *22*). It is the increase in transcription that likely compensates early in life for the accumulation of unprocessed transcripts because we do not see obvious changes in OXPHOS function or stabilization of the steady-state levels of several nuclear- and mitochondrial-encoded OXPHOS polypeptides, despite defects in de novo mitochondrial protein synthesis. However, with

age, we found that OXPHOS function and levels in the *Ptcd1* heterozygous mice are lowered, and their mitochondria are uncoupled as a consequence of persistent imbalance in mt-RNA processing and decreased protein synthesis. We found that there were more severe molecular defects in liver mitochondria compared to heart mitochondria of *Ptcd1* heterozygous mice even with age, possibly reflecting the differences in mitochondrial transcript abundance as a result of the energy demands of these tissues. The heart is a postmitotic tissue and has excess mt-RNA (*24*) that may enable it to cope with sudden changes in energy demands over a short period of time. In contrast, the liver is a highly proliferative tissue and mt-RNA accounts for ~12% of total liver RNA, possibly leaving this tissue little capacity to deal with disturbances in mitochondrial translation and protein levels during development or changes in energy demands.

The reduction in ATP synthase and complex III levels in the *Ptcd1* heterozygous mice is a direct consequence of the decreased protein synthesis in these mice, and this is more obvious with age. Because the ATP synthase and respiratory complexes have been shown to play a role in the formation and maintenance of the mitochondrial inner membrane cristae morphology (*27*, *40*–*42*), it is possible that the reduction of PTCD1 and downstream consequences on the OXPHOS system and ATP levels, albeit mild, could be sufficient to induce stress and cleavage of OPA1, thereby leading to the accumulation of the S-OPA1. The balance in the levels of S-OPA1 and L-OPA1 is important for maintaining normal cristae morphology (*43*), where increased levels of S-OPA1 can cause mitochondrial cristae remodeling (*44*, *45*) that leads to disease, as we have observed here in the livers of the heterozygous *Ptcd1* mice. In addition, reduction in OPA1 has been shown to play a role in mitochondrial dysfunction and late-onset cardiomyopathy (*46*), similar to the adult-onset cardiac dysfunction in the $Ptcd1^{+/-}$ mice. Mice lacking OMA-1, the processing peptidase of OPA1, result in imbalanced distribution of the OPA1 isoforms and suffer from changes in metabolic function that lead to decreased energy expenditure, increased adipose mass, and reduced thermogenesis and transcriptional changes in the glucose metabolism pathways and cause obesity and hepatic steatosis (*44*, *47*). We also found that the levels of large mitochondrial ribosomal subunit proteins were decreased, which may affect the assembly of the large ribosomal subunit as a consequence of changes in the inner membrane and cristae because the large ribosomal subunit is anchored to the mitochondrial inner membrane. In our model, for the first time to our knowledge, we show that changes in mitochondrial gene expression can initiate defects that affect OPA1 processing with similar metabolic consequences involving increased fat deposition, cardiomyopathy, and hepatic steatosis. Our model indicates that balanced regulation of mitochondrial gene expression can be tissue-specific, and mt-RNA defects can have varying impact depending on the energy demands of tissues.

The MICOS complex plays an important role in cristae organization and morphology required for mitochondrial biogenesis (*48*, *49*). Although the levels of most MICOS proteins associated with the inner mitochondrial membrane were not changed in the heterozygous mice, the CHCHD3 protein was increased in the heterozygous mice. CHCHD3 associates with OPA1(*29*), and it is possible that the increased levels are a compensatory response to the accumulation of S-OPA1, in an effort to counteract cristae remodeling, suggesting that OPA1 changes can be sensed by MICOS via the CHCHD3 protein.

Changes in mitochondrial morphology and consequent dysfunction can lead to metabolic changes, including insulin resistance and obesity (*47*), as well as changes in mTOR signaling (*44*). Here, we show that impaired mitochondrial gene expression and biogenesis can cause tissue-specific changes in mTOR signaling, perturbed fatty acid metabolism, and consequently glucose intolerance and inflammation. In the liver of *Ptcd1* heterozygous mice, when ATP levels are decreased, the energy and nutrient sensor AMPKα is activated by phosphorylation, which inhibits the activation of mTOR. This phenomenon has been observed previously, where decrease in hepatic mTOR and mTORC1 activity results in a fragmented mitochondrial network, and a drop in cristae density that is associated with reduction in mitochondrial respiratory capacity decreases L-OPA1 (*44*). In contrast, mTOR signaling is up-regulated via mTORC1 in the hearts of *Ptcd1* heterozygous mice, resulting in increased phosphorylation of S6 and 4E-BP1, indicating that this tissue can cope with mitochondrial dysfunction by increasing cytoplasmic protein synthesis. This may be a coping mechanism for mitochondrial dysfunction in postmitotic tissues, such as heart and muscle, because it has been found in other models of mitochondrial disease caused by defects in OXPHOS biogenesis (*35*). The increase in mTOR signaling in the heart is consistent with decreased phosphorylation of AMPKα and relatively normal ATP levels. The tissue-specific differences in mTOR signaling likely reflect their different energy demands, because mTOR has been shown to respond directly to changes in ATP levels (*50*) such that the liver inhibits mTOR signaling as a means to preserve energy expenditure that is not present in excess, whereas the heart up-regulates mTOR signaling to cope with potential decline in mitochondrial OXPHOS.

The metabolic changes in response to impaired RNA metabolism and biogenesis were consistent with changes in hormones associated with obesity, mitochondrial dysfunction, as well as cardiac and liver injury. Leptin is secreted by adipose tissue and regulates body weight, food intake, and energy expenditure by interacting with appetite and satiety centers in the brain (*51*). The increase in leptin levels correlates with increased body weight and fat deposits (*52*), and these are consistent in the obese $Ptcd1^{+/-}$ mice. Increase in FGF-21 in the $Ptcd1^{+/-}$ mice was in response to mitochondrial dysfunction and the development of cardiomyopathy, because increase in FGF-21 is commonly used as a biomarker of mitochondrial dysfunction and disease involving cardiac and skeletal muscle defects (*32*, *33*). These effects are consistent with a recent report showing that an increase in FGF-21 in obese animals represses mTORC1 in the liver, which reduces the ability of hepatic mTOR to regulate carbohydrate and lipid metabolism (*53*). The immunomodulating cytokine IL-6 has roles in inflammation, metabolism, and the activation of AMPKα (*54*), and mice lacking IL-6 have adult-onset obesity, liver steatosis, and insulin resistance (*55*–*57*). The increase in IL-6 seen in our mice indicates that this cytokine has a proinflammatory role stimulating increased phosphorylation of JNK that causes chronic hepatic injury, lipid accumulation, liver steatosis, and insulin resistance. Increased inflammation caused by sustained JNK phosphorylation can negatively regulate the insulin receptor (*56*), which may underlie the insulin resistance observed in our adult obese $Ptcd1^{+/-}$ mice. Mitochondrial dysfunction resulting from chronic inflammation has been shown to induce lipid accumulation (*58*), whereas IL-6 enhances hepatic triglyceride and glucose levels, thereby exerting pathogenicity in age-related disease (*59*). Leptin, FGF-21, and IL-6 levels are increased from a young age in the $Ptcd1^{+/-}$ mice, suggesting that these hormones respond early in life to imbalanced RNA metabolism and biogenesis and act as biomarkers for age-induced obesity, mitochondrial dysfunction–induced heart disease, and inflammation.

Changes in mitochondrial gene expression and consequent mitochondrial dysfunction as a result of point mutations in mt-RBPs cause

pathology in different tissues with varying severity in human disease (*3*, *60*) and mouse models of disease (*61*, *62*). The *Ptcd1* heterozygous mice have multiple pathologies, indicating that PTCD1 reduction is sufficient to cause increased fractional shortening in the heart and chronic injury, lipid accumulation, and fibrosis in the liver. Compromised mitochondrial biogenesis, uncoupling of OXPHOS, and consequent morphology changes, sustained over time, cause a metabolic switch possibly from fatty acid utilization to glucose metabolism in the adult *Ptcd1* heterozygous mice, which has been shown to play a critical role in the development of late-onset cardiomyopathy in *Yme1l* knockout mice (*45*). Increase in fatty acids and consequent accumulation of fat in the liver caused the development of steatosis and inflammation in the *Ptcd1* heterozygous mice. This chronic liver injury leads to an increase in the number of liver progenitor cells in an effort to repair liver function (*63*).

Our work here identifies PTCD1 as an essential protein for mitochondrial biogenesis and metabolic function in vivo. Although PTCD1 levels in cells are relatively low, its expression from both alleles is required for mitochondrial function and structure. Reduction of PTCD1 leads to adult-onset metabolic reprogramming as a result of reduced OXPHOS function and mitochondrial uncoupling that have downstream effects on insulin and mTOR signaling pathways and fatty acid metabolism, which are exacerbated with age to cause disease. Our findings provide an important model that experimentally demonstrates how haploinsufficiency can play a significant role in the predisposition to metabolic syndrome and obesity in adulthood. More importantly, we show that even minor perturbations in mt-RNA metabolism and decreased mitochondrial protein synthesis are sufficient to cause late-onset disease and a significant impact on energy metabolism. Future work should focus on functional analyses of heterozygous loss of function as a result of mutations that can cause human metabolic diseases, obesity, and diabetes to understand which single-nucleotide variants identified in large cohorts are the functional contributors to these diseases.

MATERIALS AND METHODS

Animals and housing

Ptcd1 transgenic mice on a C57BL/6N background were generated by the Australian Phenomics Network (APN; Monash University, Melbourne, Australia). ES cells harboring a start codon to stop codon *Ptcd1* knockout allele (*Ptcd1*$^{tm1(KOMP)Vlcg}$) were obtained from the Knockout Mouse Project (KOMP) Repository (University of California, Davis, CA). Blastocysts were injected with ES cells and transferred to pseudopregnant recipient mice. Mice chimeric for the *Ptcd1* knockout allele were bred with wild-type C57BL/6N mice to obtain heterozygote offspring. Male age- and littermate-matched wild-type (*Ptcd1*$^{+/+}$) and heterozygous (*Ptcd1*$^{+/-}$) mice were housed in standard cages (45 cm × 29 cm × 12 cm) under a 12-hour light/dark schedule (lights on 7 a.m. to 7 p.m.) in controlled environmental conditions of 22 ± 2°C and 50 + 10% relative humidity and fed a NCD (Rat and Mouse Chow, Specialty Feeds), and water was provided ad libitum. All studies were performed in animals aged 5 to 30 weeks unless otherwise specified. The study was approved by the Animal Ethics Committee of the University of Western Australia and performed in accordance with Principles of Laboratory Care (National Health and Medical Research Council, *Australian Code for the Care and Use of Animals for Scientific Purposes*, ed. 8, 2013).

Tissue homogenate preparation

Tissue pieces (liver and heart) (3 mm × 3 mm) were ground into a fine powder using a mortar and pestle in liquid N_2 and homogenized in 100 μl of cell extraction buffer [100 mM tris, 2 mM Na_3VO_4, 100 mM NaCl, 1% Triton X-100, 1 mM EDTA, 10% glycerol, 1 mM EGTA, 0.1% SDS, 1 mM NaF, 0.5% deoxycholate, 20 mM $Na_4P_2O_7$ (pH 7.4)], containing PhosSTOP phosphatase inhibitor cocktail (Roche) and EDTA-free cOmplete protease inhibitor cocktail (Roche). The homogenate was centrifuged at 10,000*g* for 5 min at 4°C. The previous steps were repeated until a clear tissue homogenate was produced. The tissue homogenate protein concentration was quantified using the bicinchoninic acid (BCA) assay using bovine serum albumin (BSA) as a standard.

Mitochondrial isolation

Mitochondria were collected from homogenized hearts and livers and isolated by differential centrifugation as described previously (*12*) with some modifications. Livers were homogenized in buffer containing 250 mM sucrose, 5 mM tris, and 1 mM EGTA (pH 7.4) with EDTA-free cOmplete protease inhibitor cocktail (Roche), and hearts were first incubated in 210 mM mannitol, 70 mM sucrose, 10 mM tris, and 0.1 mM EDTA (pH 7.4) containing EDTA-free cOmplete protease inhibitor cocktail (Roche) for 10 min before homogenization and differential centrifugation. The mitochondrial protein concentration was quantified using the BCA assay using BSA as a standard.

RNA isolation and Northern blotting

RNA was isolated from total hearts or heart mitochondria using the miRNeasy Mini Kit (Qiagen) incorporating an on-column RNase-free deoxyribonuclease digestion to remove all DNA. RNA (5 μg) was resolved on 1.2% agarose formaldehyde gels, then transferred to 0.45-μm Hybond-N^+ nitrocellulose membrane (GE Life Sciences), and hybridized with biotinylated oligonucleotide probes specific to mouse mitochondrial mRNAs, rRNAs, and tRNAs (*16*). Hybridizations were carried out overnight at 50°C in 5× SSC, 20 mM Na_2HPO_4, 7% SDS, and heparin (100 μg/ml), followed by washing. The signal was detected using streptavidin-linked infrared-labeled antibody [diluted 1:2000 in 3× SSC, 5% SDS, and 25 mM Na_2HPO_4 (pH 7.5)] using an Odyssey Infrared Imaging System (LI-COR Biosciences).

RNA-Seq and alignments

RNA-seq was performed on total RNA from three control and three *Ptcd1* heterozygous mice by the Australian Genomic Research Facility on the Illumina NextSeq platform, according to the Illumina TruSeq protocol. We used random hexamer primers for cDNA library generation and performed cytoplasmic rRNA depletion using the Ribo-Zero rRNA removal kit. Adapter trimming was performed by cutadapt (*64*). To analyze the mitochondrial transcriptome, sequenced single end reads were initially aligned to the mouse genome (mm10) with HISAT2 v2.0.4 (NUMTs masked) (*65*). The read IDs of all mitochondrial primary alignments were extracted with SAMtools v1.3 (*66*) and used to filter the original alignments into nuclear and mitochondrial alignment files with Picard v1.23 (http://broadinstitute.github.io/picard/). The mitochondrial alignments were converted back to their original read sequence in FASTQ format with Picard and realigned to the mitochondrial genome as before with the additional parameter --no-spliced-alignment. Primary mitochondrial alignments were extracted and separated according to their template strand of origin with SAMtools and converted to template strand-specific fragment BED files with BEDtools (*67*) and ad hoc scripts. Per-base depth of strand-specific fragment BED files was generated with BEDtools normalized by the total number of properly mapped reads per million across the whole genome (nuclear and mitochondrial) and converted to bedGraph

format for visualization with Integrative Genomics Viewer v2.3.9 (*68*, *69*).

Immunoblotting

Specific proteins were detected using rabbit monoclonal antibodies against RG9MTD1 (HPA036671), HSD17B70 (HPA001432), and MRPS34 (HPA042112) (Sigma—Prestige Antibodies, diluted 1:500); MRPS35 (16457-1-AP), MRPL44 (16394-1-AP), MRPL37 (15190-1-AP), MRPS16 (16735-1-AP), MRPL11 (15543-1-AP), and AFG3L2 (14631-1-AP) (Proteintech, diluted 1:1000); phosphorylated (Ser^{2448}; 5535) and nonphosphorylated mTOR (2983), phosphorylated (Thr^{183}/Tyr^{185}; 4668) and nonphosphorylated SAPK/JNK (9252), phosphorylated (Thr^{172}; 2532) and nonphosphorylated AMPKα (2532), phosphorylated (Ser^{473}; 4051) and nonphosphorylated Akt (9272), phosphorylated ($Ser^{235/236}$; 4856) and nonphosphorylated S6 (2217), phosphorylated ($Thr^{37/36}$; 2855) and nonphosphorylated 4E-BP-1 (9644), Rictor (2140), ACC (3662), and GAPDH (2118) (Cell Signaling Technology, diluted 1:500); Raptor (ab40768), PGC-1 (ab54481), and YY1 (ab109228) (Abcam, diluted 1:1000); and CHCHD3 (OAEB01622) (Aviva Systems Biology, diluted 1:500). Specific rabbit polyclonal antibodies were used against PTCD1 (H116; sc-382428) (Santa Cruz Biotechnology, diluted 1:250), TFAM (ab131607) (Abcam, diluted 1:200), ELAC2 (10061-1-AP) and OMA-1 (17116-1-AP) (Proteintech, diluted 1:200), APOOL (OAAF03292) and ACACA (pACC Ser^{79}; OAAN02936) (Aviva Systems Biology, diluted 1:200), and LRP130 (sc-166177) (Santa Cruz Biotechnology, diluted 1:500). Specific mouse monoclonal antibodies used were Total OXPHOS Cocktail Antibody (ab110412), NDUFA9 (ab14714), SDHA (ab14715), UQCRC2 (ab14745), COXI (ab14705), COXII (ab198286), COXIII (ab110259), COXIV (ab14744), ATP5a (ab14748), ATP inhibitory factor 1 (ab110277), and OPA1 (ab42364) (Abcam, diluted 1:1000) and APOO (OAAB09635) (Aviva Systems Biology, diluted 1:200) in Odyssey blocking buffer (LI-COR Biosciences). IRDye 800CW goat anti-rabbit immunoglobulin G (IgG) or IRDye 680LT goat anti-mouse IgG (LI-COR Biosciences) secondary antibodies were used, and the immunoblots were visualized using an Odyssey infrared imaging system (Li-COR Biosciences).

BN-PAGE and in-gel activity staining

BN-PAGE was performed using isolated mitochondria from hearts and livers, as described previously (*12*). BN-PAGE gels were analyzed by in-gel activity assays or by transferring to polyvinylidene difluoride and immunoblotting against the respiratory complexes. In-gel enzyme activity assays were performed for mitochondrial complex V after BN-PAGE. The gel was soaked in 50 mM glycine/NaOH buffer (pH 8.6) for 1 hour at room temperature before incubation in 50 mM glycine, 0.05% lead acetate, 5 mM $MgCl_2$, and 5 mM ATP (pH 8.6) at 37°C until white bands appeared on the gel.

Translation assay

In organello translation assays were carried out in isolated heart and liver mitochondria, as described previously (*12*). Briefly, 500 μg of mitochondria was incubated in 750 μl of translation buffer [100 mM mannitol, 10 mM sodium succinate, 80 mM KCl, 5 mM $MgCl_2$, 1 mM KPi, 25 mM Hepes (pH 7.4), 5 mM ATP, 20 μM guanosine triphosphate, 6 mM creatine phosphate, creatine kinase (60 μg/ml), and 60 μg/ml of all amino acids except methionine]. Mitochondria were supplemented with 150 μCi of [^{35}S]methionine (PerkinElmer) for 60 min at 37°C. After labeling, mitochondria were washed in translation buffer and suspended in radioimmunoprecipitation assay lysis buffer. Protein concentration was measured, and 50 μg of mitochondrial protein was resolved by SDS-PAGE and visualized by autoradiography.

Respiration and membrane potential measurements

Mitochondrial respiration was evaluated as O_2 consumption in isolated heart and liver mitochondria, as previously described (*12*). Mitochondria were supplemented with substrates 10 mM glutamate/2 mM malate (Sigma), 10 mM succinate/0.5 μM rotenone (Sigma), or 1 mM tetramethyl-*p*-phenylenediamine/1 mM ascorbate (Sigma). After addition of 1 mM ADP (Sigma) to the recording chamber, state 3 respiration activity was measured. ADP-independent respiration activity (state 4) was monitored after addition of antimycin A (2 mM, Sigma). Respiration was uncoupled by successive addition of FCCP up to 3 μM to reach maximal respiration. Mitochondrial membrane potential in isolated mitochondria and MEFs was measured as described previously (*70*).

Cell culture and fluorescence microscopy

MEFs were cultured at 37°C under humidified 95% air/5% CO_2 in Dulbecco's modified Eagle's medium (Gibco, Life Technologies) containing glucose (4.5 g/liter or 1 g/liter), 2 mM glutamine, penicillin (100 U/ml), streptomycin sulfate (100 μg/ml), and 10% fetal bovine serum or galactose (1 g/liter). MEFs were plated onto 13-mm-diameter glass coverslips and allowed to attach overnight. Cells were treated with 100 nM MitoTracker Orange for 15 min and then washed with tris-buffered saline [5 mM tris-HCl (pH 7.4) and 20 mM NaCl] before mounting in 1,4-diazabicyclo-octane/polyvinyl alcohol medium. Images were acquired using an Olympus IX71 inverted microscope using an Olympus 60× objective.

Echocardiography

ECG was performed on $Ptcd1^{+/+}$ and $Ptcd1^{+/-}$ aged mice under light methoxyflurane anesthesia with the use of an i13L probe on a Vivid 7 Dimension (GE Healthcare), as described previously (*61*).

Histology

Fresh sections of the liver and heart tissues were frozen in optimal cutting temperature medium or fixed in 10% neutral-buffered formalin, then embedded in paraffin wax, sectioned in 5- to 10-μm sections, and stained with H&E and Oil red O and hematoxylin. Images were acquired using a Nikon Ti Eclipse inverted microscope using a Nikon 20× objective, and staining was quantified as described previously (*61*).

Metabolic studies

An intraperitoneal GTT and ITT were performed on mice that were fasted for 5 hours. Blood samples were obtained from the tail tip at 0, 15, 30, 45, 60, 90, and 120 min after glucose or insulin injection. Blood glucose levels were measured using a glucometer (Accu-Chek Inform a II, Roche). During these tests, glucose (1 g/kg) and insulin (0.5 U/kg) were used for GTT and ITT, respectively. Cardiac blood samples were taken to measure insulin, IL-6, leptin (Merck Millipore), and FGF-21 (R&D Systems) using standard ELISA kits according to the manufacturer's instructions. Data were analyzed using an online software program (www.elisaanalysis.com), and the area under the curve was calculated using the trapezoidal rule with Microsoft Excel. Serum triglyceride and cholesterol levels were measured by PathWest Laboratory of Medicine. ADP/ATP ratio was determined using a commercially available bioluminescent kit according to the manufacturer's instructions (Abcam).

Transmission electron microscopy

Tissue preparation and imaging for *Ptcd1*$^{+/+}$ and *Ptcd1*$^{+/-}$ heart and liver tissue were performed as described previously (*71*).

SUPPLEMENTARY MATERIALS

Supplementary material for this article is available at http://advances.sciencemag.org/cgi/content/full/3/8/e1700677/DC1

fig. S1. The effects of PTCD1 loss on embryo development.
fig. S2. Transcriptome-wide analyses of RNA processing in liver mitochondria by RNA-Seq.
fig. S3. Transcriptome-wide analyses of RNA processing in heart mitochondria by RNA-Seq.
fig. S4. The effects of PTCD1 reduction on mitochondrial function in 40-week-old mice.
fig. S5. The effects of PTCD1 reduction on mitochondrial function in 10-week-old mice.
fig. S6. Reduction in PTCD1 affects the mitochondrial membrane potential.

REFERENCES AND NOTES

1. O. Rackham, T. R. Mercer, A. Filipovska, The human mitochondrial transcriptome and the RNA-binding proteins that regulate its expression. *Wiley Interdiscip. Rev. RNA* **3**, 675–695 (2012).
2. B. M. Hällberg, N.-G. Larsson, Making proteins in the powerhouse. *Cell Metab.* **20**, 226–240 (2014).
3. S. B. Vafai, V. K. Mootha, Mitochondrial disorders as windows into an ancient organelle. *Nature* **491**, 374–383 (2012).
4. A. Barkan, M. Rojas, S. Fujii, A. Yap, Y. S. Chong, C. S. Bond, I. Small, A combinatorial amino acid code for RNA recognition by pentatricopeptide repeat proteins. *PLOS Genet.* **8**, e1002910 (2012).
5. A. Filipovska, O. Rackham, Designer RNA-binding proteins: New tools for manipulating the transcriptome. *RNA Biol.* **8**, 978–983 (2011).
6. I. D. Small, O. Rackham, A. Filipovska, Organelle transcriptomes: Products of a deconstructed genome. *Curr. Opin. Microbiol.* **16**, 652–658 (2013).
7. O. Rackham, A. Filipovska, The role of mammalian PPR domain proteins in the regulation of mitochondrial gene expression. *Biochim. Biophys. Acta* **1819**, 1008–1016 (2011).
8. S. M. K. Davies, M. I. G. Lopez Sanchez, R. Narsai, A.-M. J. Shearwood, M. F. M. Razif, I. D. Small, J. Whelan, O. Rackham, A. Filipovska, MRPS27 is a pentatricopeptide repeat domain protein required for the translation of mitochondrially encoded proteins. *FEBS Lett.* **586**, 3555–3561 (2012).
9. S. M. K. Davies, O. Rackham, A.-M. J. Shearwood, K. L. Hamilton, R. Narsai, J. Whelan, A. Filipovska, Pentatricopeptide repeat domain protein 3 associates with the mitochondrial small ribosomal subunit and regulates translation. *FEBS Lett.* **583**, 1853–1858 (2009).
10. I. Kühl, M. Miranda, V. Posse, D. Milenkovic, A. Mourier, S. J. Siira, N. A. Bonekamp, U. Neumann, A. Filipovska, P. L. Polosa, C. M. Gustafsson, N.-G. Larsson, POLRMT regulates the switch between replication primer formation and gene expression of mammalian mtDNA. *Sci. Adv.* **2**, e1600963 (2016).
11. I. Kühl, C. Kukat, B. Ruzzenente, D. Milenkovic, A. Mourier, M. Miranda, C. Koolmeister, M. Falkenberg, N.-G. Larsson, POLRMT does not transcribe nuclear genes. *Nature* **514**, E7–E11 (2014).
12. O. Rackham, J. D. Busch, S. Matic, S. J. Siira, I. Kuznetsova, I. Atanassov, J. A. Ermer, A.-M. J. Shearwood, T. R. Richman, J. B. Stewart, A. Mourier, D. Milenkovic, N.-G. Larsson, A. Filipovska, Hierarchical RNA processing is required for mitochondrial ribosome assembly. *Cell Rep.* **16**, 1874–1890 (2016).
13. B. Ruzzenente, M. D. Metodiev, A. Wredenberg, A. Bratic, C. B. Park, Y. Cámara, D. Milenkovic, V. Zickermann, R. Wibom, K. Hultenby, H. Erdjument-Bromage, P. Tempst, U. Brandt, J. B. Stewart, C. M. Gustafsson, N.-G. Larsson, LRPPRC is necessary for polyadenylation and coordination of translation of mitochondrial mRNAs. *EMBO J.* **31**, 443–456 (2012).
14. F. Sasarman, C. Brunel-Guitton, H. Antonicka, T. Wai, E. A. Shoubridge, LRPPRC and SLIRP interact in a ribonucleoprotein complex that regulates posttranscriptional gene expression in mitochondria. *Mol. Biol. Cell* **21**, 1315–1323 (2010).
15. F. Xu, C. Ackerley, M. C. Maj, J. B. L. Addis, V. Levandovskiy, J. Lee, N. MacKay, J. M. Cameron, B. H. Robinson, Disruption of a mitochondrial RNA-binding protein gene results in decreased cytochrome *b* expression and a marked reduction in ubiquinol–cytochrome *c* reductase activity in mouse heart mitochondria. *Biochem. J.* **416**, 15–26 (2008).
16. O. Rackham, S. M. K. Davies, A.-M. J. Shearwood, K. L. Hamilton, J. Whelan, A. Filipovska, Pentatricopeptide repeat domain protein 1 lowers the levels of mitochondrial leucine tRNAs in cells. *Nucleic Acids Res.* **37**, 5859–5867 (2009).
17. M. I. G. Lopez Sanchez, T. R. Mercer, S. M. K. Davies, A.-M. J. Shearwood, K. K. A. Nygård, T. R. Richman, J. S. Mattick, O. Rackham, A. Filipovska, RNA processing in human mitochondria. *Cell Cycle* **10**, 2904–2916 (2011).
18. G. Liu, T. R. Mercer, A.-M. J. Shearwood, S. J. Siira, M. E. Hibbs, J. S. Mattick, O. Rackham, A. Filipovska, Mapping of mitochondrial RNA-protein interactions by digital RNase footprinting. *Cell Rep.* **5**, 839–848 (2013).
19. N.-G. Larsson, J. Wang, H. Wilhelmsson, A. Oldfors, P. Rustin, M. Lewandoski, G. S. Barsh, D. A. Clayton, Mitochondrial transcription factor A is necessary for mtDNA maintenance and embryogenesis in mice. *Nat. Genet.* **18**, 231–236 (1998).
20. C. B. Park, J. Asin-Cayuela, Y. Cámara, Y. Shi, M. Pellegrini, M. Gaspari, R. Wibom, K. Hultenby, H. Erdjument-Bromage, P. Tempst, M. Falkenberg, MTERF3 is a negative regulator of mammalian mtDNA transcription. *Cell* **130**, 273–285 (2007).
21. M. D. Metodiev, H. Spåhr, P. L. Polosa, C. Meharg, C. Becker, J. Altmueller, B. Habermann, N.-G. Larsson, B. Ruzzenente, NSUN4 is a dual function mitochondrial protein required for both methylation of 12S rRNA and coordination of mitoribosomal assembly. *PLOS Genet.* **10**, e1004110 (2014).
22. M. Metodiev, N. Lesko, C. B. Park, Y. Cámara, Y. Shi, R. Wibom, K. Hultenby, C. M. Gustafsson, N.-G. Larsson, Methylation of 12S rRNA is necessary for in vivo stability of the small subunit of the mammalian mitochondrial ribosome. *Cell Metab.* **9**, 386–397 (2009).
23. Y. Y. Cámara, J. Asin-Cayuela, C. B. Park, M. D. Metodiev, Y. Shi, B. Ruzzenente, C. Kukat, B. Habermann, R. Wibom, K. Hultenby, T. Franz, H. Erdjument-Bromage, P. Tempst, B. M. Hallberg, C. M. Gustafsson, N.-G. Larsson, MTERF4 regulates translation by targeting the methyltransferase NSUN4 to the mammalian mitochondrial ribosome. *Cell Metab.* **13**, 527–539 (2011).
24. T. R. Mercer, S. Neph, M. E. Dinger, J. Crawford, M. A. Smith, A.-M. J. Shearwood, E. Haugen, C. P. Bracken, O. Rackham, J. A. Stamatoyannopoulos, A. Filipovska, J. S. Mattick, The human mitochondrial transcriptome. *Cell* **146**, 645–658 (2011).
25. S. Cipolat, O. M. de Brito, B. D. Zilio, L. Scorrano, OPA1 requires mitofusin 1 to promote mitochondrial fusion. *Proc. Natl. Acad. Sci. U.S.A.* **101**, 15927–15932 (2004).
26. T. MacVicar, T. Langer, OPA1 processing in cell death and disease—The long and short of it. *J. Cell Sci.* **129**, 2297–2306 (2016).
27. S. Cogliati, C. Frezza, M. E. Soriano, T. Varanita, R. Quintana-Cabrera, M. Corrado, S. Cipolat, V. Costa, A. Casarin, L. C. Gomes, E. Perales-Clemente, L. Salviati, P. Fernandez-Silva, J. A. Enriquez, L. Scorrano, Mitochondrial cristae shape determines respiratory chain supercomplexes assembly and respiratory efficiency. *Cell* **155**, 160–171 (2013).
28. I. Bohovych, M. R. Fernandez, J. J. Rahn, K. D. Stackley, J. E. Bestman, A. Anandhan, R. Franco, S. M. Claypool, R. E. Lewis, S. S. L. Chan, O. Khalimonchuk, Metalloprotease OMA1 fine-tunes mitochondrial bioenergetic function and respiratory supercomplex stability. *Sci. Rep.* **5**, 13989 (2015).
29. M. Darshi, V. L. Mendiola, M. R. Mackey, A. N. Murphy, A. Koller, G. A. Perkins, M. H. Ellisman, S. S. Taylor, ChChd3, an inner mitochondrial membrane protein, is essential for maintaining crista integrity and mitochondrial function. *J. Biol. Chem.* **286**, 2918–2932 (2011).
30. T. B. Haack, R. Kopajtich, P. Freisinger, T. Wieland, J. Rorbach, T. J. Nicholls, E. Baruffini, A. Walther, K. Danhauser, F. A. Zimmermann, R. A. Husain, J. Schum, H. Mundy, I. Ferrero, T. M. Strom, T. Meitinger, R. W. Taylor, M. Minczuk, J. A. Mayr, H. Prokisch, *ELAC2* mutations cause a mitochondrial RNA processing defect associated with hypertrophic cardiomyopathy. *Am. J. Hum. Genet.* **93**, 211–223 (2013).
31. M. Giralt, A. Gavaldà-Navarro, F. Villarroya, Fibroblast growth factor-21, energy balance and obesity. *Mol. Cell. Endocrinol.* **418** (Pt. 1), 66–73 (2015).
32. S. A. Dogan, C. Pujol, P. Maiti, A. Kukat, S. Wang, S. Hermans, K. Senft, R. Wibom, E. I. Rugarli, A. Trifunovic, Tissue-specific loss of DARS2 activates stress responses independently of respiratory chain deficiency in the heart. *Cell Metab.* **19**, 458–469 (2014).
33. A. Suomalainen, Fibroblast growth factor 21: A novel biomarker for human muscle-manifesting mitochondrial disorders. *Expert Opin. Med. Diagn.* **7**, 313–317 (2013).
34. M. Morita, S.-P. Gravel, V. Chénard, K. Sikström, L. Zheng, T. Alain, V. Gandin, D. Avizonis, M. Arguello, C. Zakaria, S. McLaughlan, Y. Nouet, A. Pause, M. Pollak, E. Gottlieb, O. Larsson, J. St-Pierre, I. Topisirovic, N. Sonenberg, mTORC1 controls mitochondrial activity and biogenesis through 4E-BP-dependent translational regulation. *Cell Metab.* **18**, 698–711 (2013).
35. S. C. Johnson, M. E. Yanos, E.-B. Kayser, A. Quintana, M. Sangesland, A. Castanza, L. Uhde, J. Hui, V. Z. Wall, A. Gagnidze, K. Oh, B. M. Wasko, F. J. Ramos, R. D. Palmiter, P. S. Rabinovitch, P. G. Morgan, M. M. Sedensky, M. Kaeberlein, mTOR inhibition alleviates mitochondrial disease in a mouse model of Leigh syndrome. *Science* **342**, 1524–1528 (2013).
36. S. C. Johnson, P. S. Rabinovitch, M. Kaeberlein, mTOR is a key modulator of ageing and age-related disease. *Nature* **493**, 338–345 (2013).
37. V. K. Mootha, P. Lepage, K. Miller, J. Bunkenborg, M. Reich, M. Hjerrild, T. Delmonte, A. Villeneuve, R. Sladek, F. Xu, G. A. Mitchell, C. Morin, M. Mann, T. J. Hudson, B. Robinson, J. D. Rioux, E. S. Lander, Identification of a gene causing human cytochrome *c* oxidase deficiency by integrative genomics. *Proc. Natl. Acad. Sci. U.S.A.* **100**, 605–610 (2003).
38. M. D. Metodiev, K. Thompson, C. L. Alston, A. A. Morris, L. He, Z. Assouline, M. Rio, N. Bahi-Buisson, A. Pyle, H. Griffin, S. Siira, A. Filipovska, A. Munnich, P. F. Chinnery,

R. McFarland, A. Rötig, R. W. Taylor, Recessive mutations in *TRMT10C* cause defects in mitochondrial RNA processing and multiple respiratory chain deficiencies. *Am. J. Hum. Genet.* **98**, 993–1000 (2016).
39. W. Weraarpachai, H. Antonicka, F. Sasarman, J. Seeger, B. Schrank, J. E. Kolesar, H. Lochmüller, M. Chevrette, B. A. Kaufman, R. Horvath, E. A. Shoubridge, Mutation in *TACO1*, encoding a translational activator of COX I, results in cytochrome c oxidase deficiency and late-onset Leigh syndrome. *Nat. Genet.* **41**, 833–837 (2009).
40. I. C. Soto, F. Fontanesi, M. Valledor, D. Horn, R. Singh, A. Barrientos, Synthesis of cytochrome *c* oxidase subunit 1 is translationally downregulated in the absence of functional F_1F_0-ATP synthase. *Biochim. Biophys. Acta* **1793**, 1776–1786 (2009).
41. K. M. Davies, C. Anselmi, I. Wittig, J. D. Faraldo-Gómez, W. Kühlbrandt, Structure of the yeast F_1F_o-ATP synthase dimer and its role in shaping the mitochondrial cristae. *Proc. Natl. Acad. Sci. U.S.A.* **109**, 13602–13607 (2012).
42. P. Paumard, J. Vaillier, B. Coulary, J. Schaeffer, V. Soubannier, D. M. Mueller, D. Brèthes, J. P. di Rago, J. Velours, The ATP synthase is involved in generating mitochondrial cristae morphology. *EMBO J.* **21**, 221–230 (2002).
43. T. Landes, L. J. Emorine, D. Courilleau, M. Rojo, P. Belenguer, L. Arnauné-Pelloquin, The BH3-only Bnip3 binds to the dynamin Opa1 to promote mitochondrial fragmentation and apoptosis by distinct mechanisms. *EMBO Rep.* **11**, 459–465 (2010).
44. A. Sood, D. V. Jeyaraju, J. Prudent, A. Caron, P. Lemieux, H. M. McBride, M. Laplante, K. Tóth, L. Pellegrini, A mitofusin-2–dependent inactivating cleavage of Opa1 links changes in mitochondria *cristae* and ER contacts in the postprandial liver. *Proc. Natl. Acad. Sci. U.S.A.* **111**, 16017–16022 (2014).
45. T. Wai, J. García-Prieto, M. J. Baker, C. Merkwirth, P. Benit, P. Rustin, F. Javier Rupérez, C. Barbas, B. Ibañez, T. Langer, Imbalanced OPA1 processing and mitochondrial fragmentation cause heart failure in mice. *Science* **350**, aad0116 (2015).
46. L. Chen, T. Liu, A. Tran, X. Lu, A. A. Tomilov, V. Davies, G. Cortopassi, N. Chiamvimonvat, D. M. Bers, M. Votruba, A. A. Knowlton, OPA1 mutation and late-onset cardiomyopathy: Mitochondrial dysfunction and mtDNA instability. *J. Am. Heart Assoc.* **1**, e003012 (2012).
47. M. J. Baker, P. A. Lampe, D. Stojanovski, A. Korwitz, R. Anand, T. Tatsuta, T. Langer, Stress-induced OMA1 activation and autocatalytic turnover regulate OPA1-dependent mitochondrial dynamics. *EMBO J.* **33**, 578–593 (2014).
48. M. Harner, C. Körner, D. Walther, D. Mokranjac, J. Kaesmacher, U. Welsch, J. Griffith, M. Mann, F. Reggiori, W. Neupert, The mitochondrial contact site complex, a determinant of mitochondrial architecture. *EMBO J.* **30**, 4356–4370 (2011).
49. M. van der Laan, S. E. Horvath, N. Pfanner, Mitochondrial contact site and cristae organizing system. *Curr. Opin. Cell Biol.* **41**, 33–42 (2016).
50. P. B. Dennis, A. Jaeschke, M. Saitoh, B. Fowler, S. C. Kozma, G. Thomas, Mammalian TOR: A homeostatic ATP sensor. *Science* **294**, 1102–1105 (2001).
51. P. J. Scarpace, M. Matheny, R. L. Moore, N. Tümer, Impaired leptin responsiveness in aged rats. *Diabetes* **49**, 431–435 (2000).
52. R. C. Frederich, A. Hamann, S. Anderson, B. Löllmann, B. B. Lowell, J. S. Flier, Leptin levels reflect body lipid content in mice: Evidence for diet-induced resistance to leptin action. *Nat. Med.* **1**, 1311–1314 (1995).
53. Q. Gong, Z. Hu, F. Zhang, A. Cui, X. Chen, H. Jiang, J. Gao, X. Chen, Y. Han, Q. Liang, D. Ye, L. Shi, Y. E. Chin, Y. Wang, H. Xiao, F. Guo, Y. Liu, M. Zang, A. Xu, Y. Li, Fibroblast growth factor 21 improves hepatic insulin sensitivity by inhibiting mammalian target of rapamycin complex 1 in mice. *Hepatology* **64**, 425–438 (2016).
54. A. L. Carey, G. R. Steinberg, S. L. Macaulay, W. G. Thomas, A. G. Holmes, G. Ramm, O. Prelovsek, C. Hohnen-Behrens, M. J. Watt, D. E. James, B. E. Kemp, B. K. Pedersen, M. A. Febbraio, Interleukin-6 increases insulin-stimulated glucose disposal in humans and glucose uptake and fatty acid oxidation in vitro via AMP-activated protein kinase. *Diabetes* **55**, 2688–2697 (2006).
55. M. J. Kraakman, H. L. Kammoun, T. L. Allen, V. Deswaerte, D. C. Henstridge, E. Estevez, V. B. Matthews, B. Neill, D. A. White, A. J. Murphy, L. Peijs, C. Yang, S. Risis, C. R. Bruce, X.-J. Du, A. Bobik, R. S. Lee-Young, B. A. Kingwell, A. Vasanthakumar, W. Shi, A. Kallies, G. I. Lancaster, S. Rose-John, M. A. Febbraio, Blocking IL-6 *trans*-signaling prevents high-fat diet-induced adipose tissue macrophage recruitment but does not improve insulin resistance. *Cell Metab.* **21**, 403–416 (2015).
56. V. B. Matthews, T. L. Allen, S. Risis, M. H. S. Chan, D. C. Henstridge, N. Watson, L. A. Zaffino, J. R. Babb, J. Boon, P. J. Meikle, J. B. Jowett, M. J. Watt, J.-O. Jansson, C. R. Bruce, M. A. Febbraio, Interleukin-6-deficient mice develop hepatic inflammation and systemic insulin resistance. *Diabetologia* **53**, 2431–2441 (2010).
57. V. Wallenius, K. Wallenius, B. Ahrén, M. Rudling, H. Carlsten, S. L. Dickson, C. Ohlsson, J.-O. Jansson, Interleukin-6-deficient mice develop mature-onset obesity. *Nat. Med.* **8**, 75–79 (2002).
58. A. Hernández-Aguilera, A. Rull, E. Rodríguez-Gallego, M. Riera-Borrull, F. Luciano-Mateo, J. Camps, J. A. Menéndez, J. Joven, Mitochondrial dysfunction: A basic mechanism in inflammation-related non-communicable diseases and therapeutic opportunities. *Mediators Inflamm.* **2013**, 135698 (2013).
59. L. A. Katunga, P. Gudimella, J. T. Efird, S. Abernathy, T. A. Mattox, C. Beatty, T. M. Darden, K. A. Thayne, H. Alwair, A. P. Kypson, J. A. Virag, E. J. Anderson, Obesity in a model of gpx4 haploinsufficiency uncovers a causal role for lipid-derived aldehydes in human metabolic disease and cardiomyopathy. *Mol. Metab.* **4**, 493–506 (2015).
60. V. Boczonadi, R. Horvath, Mitochondria: Impaired mitochondrial translation in human disease. *Int. J. Biochem. Cell Biol.* **48**, 77–84 (2014).
61. T. R. Richman, J. A. Ermer, S. M. K. Davies, K. L. Perks, H. M. Viola, A.-M. J. Shearwood, L. C. Hool, O. Rackham, A. Filipovska, Mutation in MRPS34 compromises protein synthesis and causes mitochondrial dysfunction. *PLOS Genet.* **11**, e1005089 (2015).
62. T. R. Richman, H. Spåhr, J. A. Ermer, S. M. K. Davies, H. M. Viola, K. A. Bates, J. Papadimitriou, L. C. Hool, J. Rodger, N.-G. Larsson, O. Rackham, A. Filipovska, Loss of the RNA-binding protein TACO1 causes late-onset mitochondrial dysfunction in mice. *Nat. Commun.* **7**, 11884 (2016).
63. F. Grizzi, M. Chiriva-Internati, Human binucleate hepatocytes: Are they a defence during chronic liver diseases? *Med. Hypotheses* **69**, 258–261 (2007).
64. M. Martin, Cutadapt removes adapter sequences from high-throughput sequencing reads. *EMBnet J.* **17**, 10–12 (2011).
65. M. Pertea, D. Kim, G. M. Pertea, J. T. Leek, S. L. Salzberg, Transcript-level expression analysis of RNA-seq experiments with HISAT, StringTie and Ballgown. *Nat. Protoc.* **11**, 1650–1667 (2016).
66. H. Li, B. Handsaker, A. Wysoker, T. Fennell, J. Ruan, N. Homer, G. Marth, G. Abecasis, R. Durbin; 1000 Genome Project Data Processing Subgroup, The sequence alignment/map format and SAMtools. *Bioinformatics* **25**, 2078–2079 (2009).
67. A. R. Quinlan, I. M. Hall, BEDTools: A flexible suite of utilities for comparing genomic features. *Bioinformatics* **26**, 841–842 (2010).
68. J. T. Robinson, H. Thorvaldsdóttir, W. Winckler, M. Guttman, E. S. Lander, G. Getz, J. P. Mesirov, Integrative genomics viewer. *Nat. Biotechnol.* **29**, 24–26 (2011).
69. H. Thorvaldsdóttir, J. T. Robinson, J. P. Mesirov, Integrative Genomics Viewer (IGV): High-performance genomics data visualization and exploration. *Brief. Bioinform.* **14**, 178–192 (2013).
70. M. M. Jellicoe, S. J. Nichols, B. A. Callus, M. V. Baker, P. J. Barnard, S. J. Berners-Price, J. Whelan, G. C. Yeoh, A. Filipovska, Bioenergetic differences selectively sensitize tumorigenic liver progenitor cells to a new gold(I) compound. *Carcinogenesis* **29**, 1124–1133 (2008).
71. H. M. Viola, V. P. A. Johnstone, H. C. Szappanos, T. R. Richman, T. Tsoutsman, A. Filipovska, C. Semsarian, J. G. Seidman, C. E. Seidman, L. C. Hool, The role of the L-type Ca^{2+} channel in altered metabolic activity in a murine model of hypertrophic cardiomyopathy. *JACC Basic Transl. Sci.* **1**, 61–72 (2016).

Acknowledgments: We thank H. Vanyai for advice on the embryo isolation and S. Siira for advice on the bioinformatic analyses. The *Ptcd1* knockout ES cell line used for this research project was generated by the trans-NIH KOMP and obtained from the KOMP Repository (www.komp.org). NIH grants to VelociGene at Regeneron Inc. (U01HG004085) and the CSD Consortium (U01HG004080) funded the generation of gene-targeted ES cells for 8500 genes in the KOMP Program and archived and distributed by the KOMP Repository at the University of California, Davis and Children's Hospital Oakland Research Institute (U42RR024244). We thank the APN node at Monash University for ES cell blastocyst injections and breeding of the chimeric *Ptcd1* knockout mice. The APN is supported by the Australian Government Department of Education through the National Collaborative Research Infrastructure Strategy, the Super Science Initiative, and the Collaborative Research Infrastructure Scheme. We acknowledge the facilities of the Australian Microscopy and Microanalysis Research Facility at the Centre for Microscopy, Characterisation and Analysis, University of Western Australia, a facility funded by the University, State, and Commonwealth Governments. **Funding:** This project was supported by fellowships and project grants from the National Health and Medical Research Council (NHMRC) (APP1058442, APP1045677, APP1041582, APP1023460, APP1005030, APP1043978, APP1062740, and APP1002207 to A.F., O.R., and L.C.H.), Australian Research Council (to A.F. and O.R.), and the Cancer Council of Western Australia (to O.R.). K.L.P. and T.R.R. were supported by NHMRC Dora Lush Scholarships, and N.F. was supported by an Australian Postgraduate Award. **Author contributions:** O.R. and A.F. conceived the project and designed the experiments. All authors conducted and analyzed the experiments. K.L.P., O.R., and A.F. wrote the manuscript, and the other authors approved the manuscript. **Competing interests:** The authors declare that they have no competing interests. **Data and materials availability:** All data needed to evaluate the conclusions in the paper are present in the paper and/or the Supplementary Materials. Additional data related to this paper may be requested from the authors.

Submitted 8 March 2017
Accepted 21 July 2017
Published 16 August 2017
10.1126/sciadv.1700677

Citation: K. L. Perks, N. Ferreira, T. R. Richman, J. A. Ermer, I. Kuznetsova, A.-M. J. Shearwood, R. G. Lee, H. M. Viola, V. P. A. Johnstone, V. Matthews, L. C. Hool, O. Rackham, A. Filipovska, Adult-onset obesity is triggered by impaired mitochondrial gene expression. *Sci. Adv.* **3**, e1700677 (2017).